

Renewable methanol production: Understanding the interplay between storage sizing, renewable mix and dispatchable energy price

Chao Chen, Aidong Yang, René Bañares-Alcántara*

Department of Engineering Science, University of Oxford, Parks Road, Oxford OX1 3PJ, UK



ARTICLE INFO

Keywords:

Electrification
Energy storage
Renewable mix
Power dispatch
Model-based optimisation

ABSTRACT

Chemical production using renewable energies is an important element on the roadmap of industry decarbonisation. This work investigates the optimisation of renewable power supply for a fully electrified methanol process, with a focus on the interplay between renewable fix, storage sizing and the use of backup dispatchable power source. The analysis is performed using the meteorological data obtained from two locations, i.e. Kramer Junction (US) and Norderney (Germany), which have excellent solar and wind source, respectively. The minimum levelised energy cost, which is optimised in terms of renewable power generation, renewable mix and storage size, is found to be 106\$/MWh and 103\$/MWh for operations in Kramer Junction and Norderney, respectively, based on a dispatchable energy price of 230\$/MWh. This leads to a levelised methanol cost of 1490\$/tonne and 1459\$/tonne with a respective renewable penetration of 81% and 96% in the production. The correlation between renewable penetration and dispatchable energy price in the most economical scenario exhibits a two-regime behaviour: the renewable penetration increases dramatically at the beginning and then slowly approaches 100% when the dispatchable energy price is above a critical point. For a fully renewable operation, the optimised levelised energy cost is found to increase to 167\$/MWh and 114\$/MWh for Kramer Junction and Norderney, respectively. The results show the importance of the dual functionality of hydrogen in the energy storage system, which improves the overall energy efficiency.

1. Introduction

Chemical production is generally energy-intensive and is responsible for a significant portion of greenhouse gas emissions. In the EU28 context, the chemical and petrochemical industry accounts for 30.7% of the total energy consumption in the industry sectors in 2015, but only 0.6% are from renewable heating [1]. To reduce the reliance on fossil fuels, the electrification of the chemical industry is considered as a promising method as there exists a growing consensus of pathways towards clean electricity [2], i.e. generating electricity from renewable energy sources. However, one of the most significant barriers in variable renewable energy (VRE) integration is its intermittent nature, which causes a fluctuating power output in electricity generation.

There are a number of technologies and strategies to level power output from VRE, such as geographical expansion [3], diversifying resources [4], storage of surplus VRE [42] and dispatchable energy backup. Instead of levelling power output, generation curtailment is another option to improve the stability of power output from VRE through generating excess electricity [5]. The opportunities for demand-side management (DSM) are discussed in depth by Strbac [6], which is also an important way in balancing generation and demand. However, there is little room for DSM in the traditional chemical industry since most

existing chemical processes require a steady-state operation (and thus a constant load). The implementation of renewable energy storage is of special importance to large-scale industrial electrification. However, inter-seasonal storage for electricity is challenging at present. On the other hand, energy carriers in the form of chemicals, such as hydrogen (H_2) and its derivatives, can be produced using surplus renewable power, offering an effective approach to overcome the energy mismatch between VRE supply and demand [7].

Although there are several studies focusing on the electrification of the chemical industry (such as the work of Bühler et al. for a specific production process [8] and Schiffer and Manthiram for the chemical industry as a whole [9]), renewable power systems for chemical processes have been rarely explored, with a few examples such as the work of Beerbühl and Schultmann for the electricity-based ammonia production integrated with renewable energies [10]. In the past, systems with a high renewable penetration were often investigated within large scales of operation. For instance, Heide et al. studied a simplified European power system based on wind and solar power generation [11]. The authors reported the impact of excess generation on balancing needs and the importance of renewable mix, especially when the wind and solar sources exhibit opposite seasonal behaviours [12]. In a similar study,

* Corresponding author.

Abbreviations

CapEx	capital expenditure
CF	capacity factor
DSM	demand side management
ESS	energy storage system
LCOMeOH	levelised cost of MeOH
LEC	levelised energy cost
MeOH	methanol
NLP	non-linear programming
OpEx	operational expenditure
PV	photovoltaic
SOFC	solid oxide fuel cell
TFCC	total fixed capital cost
VRE	variable renewable energy
c_D	unit price of dispatchable power (\$/MWh)
C_{CW}^{ELY}	annual cost of cooling water (\$)
C_{ELY}^{ESS}	annualised cost of the electrolyzers for ESS (\$)
C_{ELY}^{pw}	annual cost of process water (\$)
C_{ELY}^{SYN}	annualised cost of the electrolyzers for MeOH synthesis (\$)
e^{ELY}	specific energy consumption of water electrolysis (kWh/kg _{H₂})
E_D	energy from dispatchable source (MWh)
E_G	energy directly from the renewable power generation (MWh)
E_{ST}	energy from the storage unit (MWh)
f_{RE}^I	renewable penetration in a load
f_{ELY}^{SYN}	fraction of load that goes to H ₂ feedstock synthesis via electrolysis
f_S	fraction of solar energy in power generation
f_W	fraction of wind energy in power generation
H	height (m)
$L(t)$	time series of storage profile (MWh or tonne of H ₂)
L^{cap}	minimum storage capacity that permits a fully renewable operation (MWh or tonne of H ₂)
L^{dv}	storage capacity as a decision variable (MWh)
M_{MeOH}	total mass of produced MeOH in a year (tonne)
n	life of a unit (years)
N	total hours in the analysis, i.e. 8760h
$P_D(t)$	time series of dispatchable power requirement (MW)
P_{ELY}^{ESS}	rated power of the electrolyzers for the ESS (MW)
\underline{P}_L	constant load requirement (MW)
\overline{P}_L	average load of a period of interest
$\underline{P}_L(t)$	variable load as a function of time
\overline{P}_S	year-average generation of solar power (MW)
$\underline{P}_S(t)$	solar power as a function of time (MW)
\overline{P}_W	year-average generation of wind power (MW)
$\underline{P}_W(t)$	wind power as a function of time (MW)
$P_\delta(t)$	hourly power mismatch normalised by load (MW)
$P_\delta^{re}(t)$	revised hourly power mismatch normalised by load (MW)
r	discount rate, i.e. 8%
t	time domain (h)
U	velocity (m/s)
z	open ground roughness level (m)
γ	excess generation factor
γ_{min}	minimum γ that permits a fully renewable operation
η_{ch}	conversion efficiency in charging mode
η_{dis}	conversion efficiency in discharging mode
σ	standard deviation

tion [13]. However, these studies lack the economic analysis, which is important as the optimal renewable mix and storage size may change when the economic feasibility is taken into consideration.

Budischak et al. investigated the cost-minimised combinations of renewable sources and electrochemical storage powering one-fifth of the US electric grid [14]. The authors reported that the electric system can be powered by 90% renewable energy at costs comparable to today's provided that 2030 estimated technology costs are used. As an example of a small scale application, Ekren et al. investigated a standalone end-user powered by a solar and wind hybrid system with battery storage, reporting the required solar and wind power size and battery capacity optimised by economic potential [15]. The above studies have a challenge in common: both demand and power generation vary during the day and the year. To use renewables to power a chemical process with a constant load, demand variation is circumvented, which however also means that there is little room for DSM. On the other hand, a chemical may be used as both an energy carrier and a feed to a chemical process; therefore, synergies may exist between energy storage and chemical production. These characteristics of powering a chemical process with renewables are yet to be studied.

Among all chemical processes, the methanol (MeOH) production through carbon dioxide (CO₂) hydrogenation has attracted broad attention in light of the importance of CO₂ valorisation [16] and the potential of MeOH as a vector to synthetic hydrocarbons [17]. Recently, Lonis et al. reported an assessment of energy systems for the production and use of renewable methanol via CO₂ hydrogenation [18]; however, the variability of renewables was not considered in their work. Gonzalez-Garay et al. have presented an insightful work by assessing the sustainability of the CO₂-based MeOH processes through multi-scale analysis from plant to planet [19]. Although the wide scope of the assessments prevails over purely economic arguments, the (renewable) power systems for their H₂ production is missing. In fact, most of the studies focusing on CO₂ hydrogenation uses a benchmark price to represent the power systems for H₂ production (such as the work of Bos et al. [20] and Nguyen and Zondervan [21]). Similarly, studies focusing on renewable H₂ production often lacks a subsequent consideration for H₂ conversion [22]. The analysis of a single system fails to convey a holistic picture of the role of renewable energy in the chemical industry. Therefore, it is pressing to explore a multi-system model with its interplay, which potentially offers new functional handles for systems optimisation.

Herein, we report the utilisation of VRE to power a fully electrified MeOH process as a case study. Filling the gaps of existing studies, this work investigates the dual functionality of H₂ (as an energy vector and a material buffer) in the renewable power system for a methanol process and its impact on the required storage capacity. The main contributions of this work are as follows: (1) it complements the previous work focusing on power-to-methanol [19] and renewable hydrogen production [22], which misses the interplay between the two production processes; (2) it demonstrates the economic potential of the power system and the MeOH plant, which are optimised by the renewable mix, excess power generation and storage capacity. Due to the added complexity, a modelling and optimisation approach has been used in this study, which is in contrast with previous studies using a scenario-based techno-economic model [23]. The optimisation framework and simplified interplay between key variables are illustrated in Fig. 1. The modelling of this work complements the previous optimisation studies of (1) renewable power systems which excludes the economics (such as the work of Heide et al. [11]) and (2) renewable chemicals which does not address the variability of renewable sources (such as the work of Esteves et al. [24] and Bos et al. [20]). The feasibility of renewable energy implementation in chemical production is evaluated taking locations (quality of renewable sources) and markets (dispatchable energy price and renewable energy costs) into account. The analysis is performed using renewable sources from two locations, namely Kramer Junction (USA) and Norderney (Germany), which have excellent solar and wind source, respectively. To investigate the synergies between systems by conjugating renewable

Rasmussen et al. investigated the synergies of storage and balancing in a pan-European power system with high levels of renewable penetra-

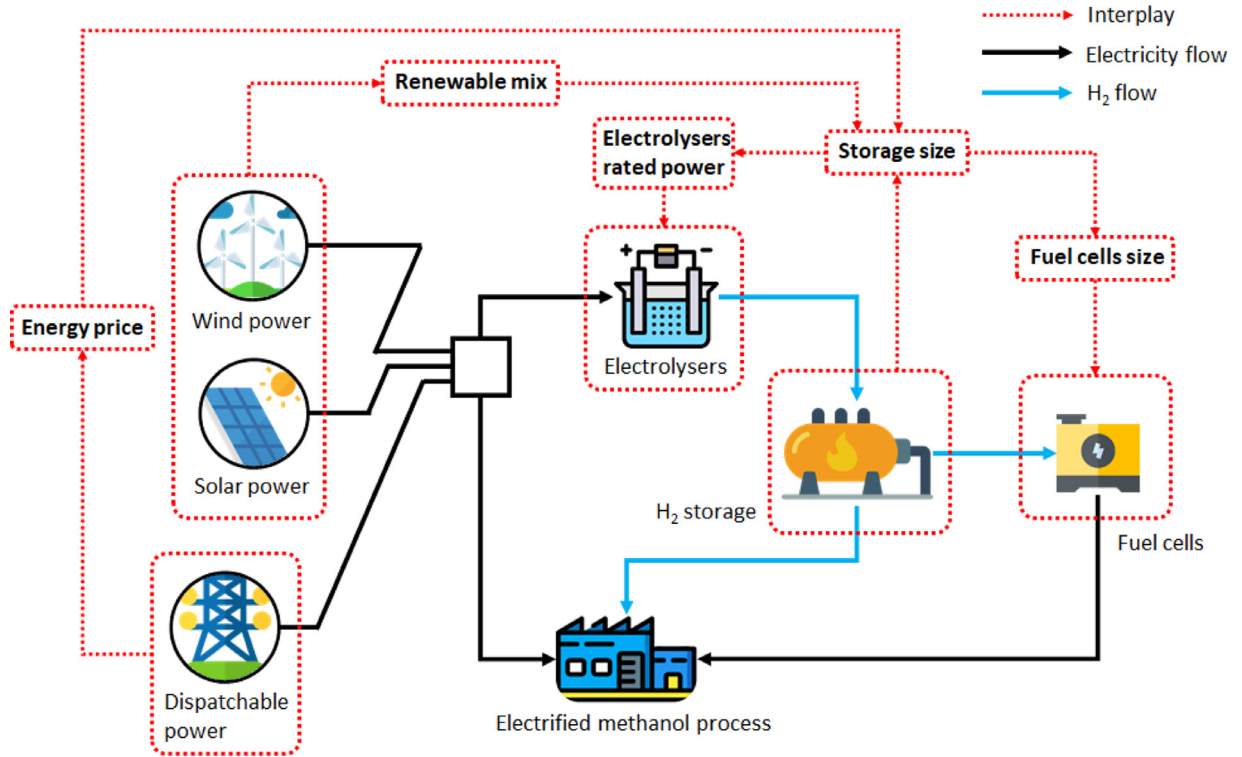


Fig. 1. Optimisation of the renewable methanol processes and a simplified illustration of the interplay between storage sizing, renewable mix and dispatchable energy price.

power generation with chemical processes is of particular significance, especially when the concepts of electrification and CO₂ valorisation are combined. As such, the optimisation results from this work would offer new insights into how the optimality is shaped collectively by the process interplay and renewable source characteristics.

2. Methods

2.1. Overview of the concept

The electrified MeOH process is adapted from our previous study [25], which consists of a MeOH synthesis loop, a carbon capture process to source CO₂ from a flue gas stream, and electrolysers for H₂ feedstock production. Note that the MeOH is synthesised via CO₂ hydrogenation to fully substitute the fossil fuel-based energy and feedstock. From the energy analysis, the electricity consumption for the fully electrified and integrated MeOH process is reported to be 12.4 kWh/kg_{MeOH} with 89% of the energy demand consumed in H₂ feed production. The detailed energy composition is illustrated in Supplementary Fig. S1. The MeOH production is designed with a constant load of 600 MW, corresponding to approximately 400,000 tonnes of MeOH per annum.

To power the chemical production using VRE, an energy storage system (ESS) is vital in order to minimise both the curtailment of generated renewable power and the reliance on dispatchable sources. The ESS is composed of alkaline electrolysers (operated at 1 atm), storage tanks of compressed H₂ (stored at 172 bar) and solid oxide fuel cells (SOFC). A SOFC has been chosen due to its relatively low cost and high efficiency. Note that, although the choice of technology does not affect the formulation of the modeling approach, it is specified since the economic analysis requires the specific and corresponding cost parameters. This work focuses on an H₂-based ESS because of its interaction with the chemical process: the stored H₂ can be fed to the MeOH synthesis directly (avoiding the fuel cells), thus increasing the overall conversion efficiency.

The analysis considers two operation scenarios, i.e. operation with and without dispatchable power backup. The former eases the constraint of storage capacity since all the remaining power mismatch (after being balanced by the ESS) would be covered by the dispatchable power. However, the inclusion of dispatchable sources increases the complexity of the scheduling, and thus an appropriate approach is required to cope with the design of the system. The latter scenario is of special interest because it features a fully renewable energy operation (all power is from the VRE or its ESS) and it is often a requirement for an operation in islanded or remote areas where dispatchable sources are not available. Although the dispatchable energy is not specified in this work, it is assumed that it is not from a renewable source. The general concept of an electrified MeOH production powered by VRE and its ESS is shown in Fig. 2. The dispatchable power backup is optional and it would only power the MeOH production, contrasting to the renewable power that would feed both the MeOH production and the ESS.

2.2. Renewable power generation

The renewable power generation consists of wind and solar power, for which the renewable mix is of special interest. To approach the problem, two base power profiles for wind ($P_W(t)$) and solar ($P_S(t)$) are defined and scaled such that the cumulative power generation throughout the period of analysis is equal to the total load, as shown in Eqs. (1) and (2):

$$\sum_{t=1}^N P_W(t) = P_L N \quad (1)$$

$$[2\pi t] \sum_{t=1}^N P_S(t) = P_L N \quad (2)$$

where P_L is the hourly load of the MeOH process and N is the total time of analysis taken as 8,760 hours, which is equivalent to one-year operation. Note that P_L is assumed as a time-invariant constant (600 MW)

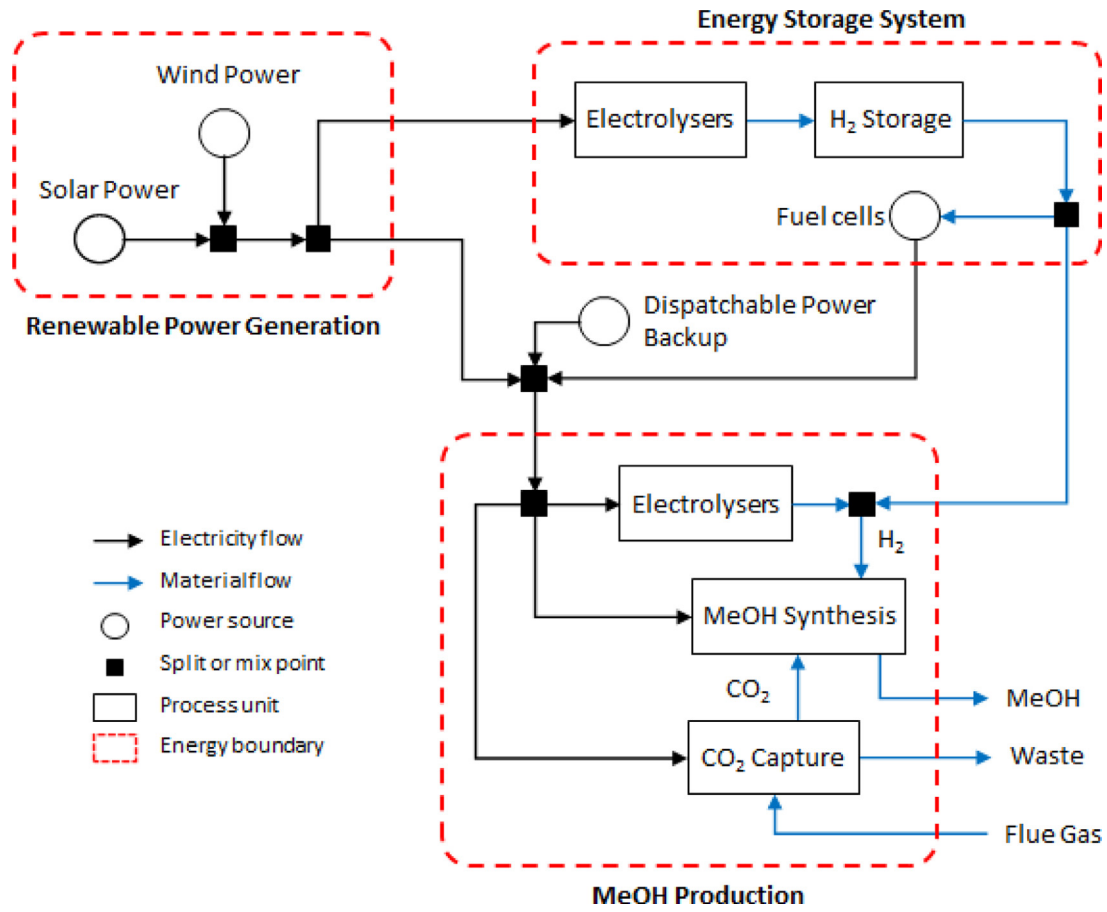


Fig. 2. Overview of the general concept for the fully electrified MeOH production powered by renewable energy and its energy storage system. The backup dispatchable power is optional.

due to the steady-state operation. The base profiles of P_W and P_S are hypothetical functions, which do not reflect the actual power generation. The conceptual profiles are adopted for modelling convenience.

Due to the intermittency of VRE, it is inevitable to generate excess renewable power in order to reliably meet the load requirement, especially when a dispatchable source is not available or too costly. Here, the over-provision factor, γ , is introduced to quantify the extent of surplus generation. Note that γ is independent of the variability of power source (in contrast to the nameplate capacity), and it only indicates the average generation relative to the load without taking the ESS into account. For example, $\gamma = 1.50$ indicates that the year-averaged combined wind and solar power generation is 1.5 times the load requirement. The mismatch (it can be either surplus or deficit) between the power generation and the load is twofold: mismatch taking or without taking the ESS into account. The time series of the power mismatch excluding the ESS is termed as $P_\delta(t)$, which is directly related to γ . This is modelled with Eq. (3):

$$P_\delta(t) = \gamma \left(f_W \frac{P_W(t)}{P_L} + f_S \frac{P_S(t)}{P_L} \right) - 1 \quad (3)$$

where f_W and f_S respectively indicate the average fraction of wind and solar power in the renewable power generation. Note that $P_\delta(t)$ is normalised by the constant load P_L . The power mismatch calculation for the cases with an ESS is introduced in Section 2.3.

A larger γ will increase the likelihood of a power surplus in the time series. Here, γ is considered as an exogenous parameter, which is usually determined by factors such as the land availability to construct the renewable energy harvesting plant and the technological or economic limitations in such a construction. Although a larger excess generation would always increase the reliability of power output, it also increases

the cost of electricity generation. In the analysis of minimum storage capacity for a fully renewable operation (i.e. no dispatchable source is required), a range of γ from 1.00 to 2.00 is analysed because the power generation would not be sufficient to fulfil the load requirement when $\gamma < 1.00$ even if the ESS is 100% efficient and any value above $\gamma = 2$ would mean an excessively over-sized and overly costly system (this has been verified in a preliminary economic analysis). For the case of using a backup dispatchable power source, the operation could be feasible when $\gamma < 1.00$ as all the remaining power deficit is met by the dispatchable source. For operations when dispatchable power sources are not available (such as islanded systems), a minimum value of excess power generation (γ_{\min}) exists in order to permit a fully renewable operation. In the economic assessment, γ is determined by optimisation.

2.3. Renewable energy storage

2.3.1. The case without dispatchable power

The storage profile of the ESS is of particular importance because it dictates the overall energy composition of the chemical process. Depending on the operation scenarios, the storage profile can be determined using different approaches. In the scenario of a fully renewable operation (all power is from VRE and its ESS), the time series of storage holdup, $L(t)$, can be calculated directly from $P_\delta(t)$: when the power mismatch is positive, the surplus VRE is stored in the ESS; when a power deficit occurs, energy is withdrawn from the ESS. However, the simple summation of positive and negative power mismatches does not represent the true storage profile as the storage capacity has to be constrained. As an illustration, the unconstrained $L(t)$ profiles are plotted in Supplementary Figs. S2 and S3. The time series of constrained storage profile

is calculated by

$$L(t) = \begin{cases} L(t-1) + \eta_{ch} P_{\delta}(t) & P_{\delta}(t) \geq 0 \\ L(t-1) + \frac{1}{\eta_{dis}} P_{\delta}(t) & P_{\delta}(t) < 0 \\ 0 & L(t-1) + \eta_{ch} P_{\delta}(t) \geq 0 \end{cases} \quad (4)$$

where η_{ch} and η_{dis} denote the conversion efficiency in charging (when $P_{\delta}(t) > 0$) and discharging (when $P_{\delta}(t) < 0$) mode, respectively. The cap value of the storage is defined as $L(t) = 0$ (a choice made for mathematical convenience), which means that at such a status the storage is full and the surplus VRE has to be curtailed. Consequently, the absolute value of $L(t)$ indicates the remaining storage capacity for charging. This approach enables the $L(t)$ profile to search for the minimum storage capacity (L^{cap}) that permits a fully renewable operation (since the dispatchable power is not available). Note that L^{cap} is specific at a given γ , f_W and location provided that $\gamma \geq \gamma_{min}$. This is because any value smaller than L^{cap} would not permit a fully renewable operation and any value larger than L^{cap} has extra storage capacity that would not be utilised (i.e. capacity wasted).

The charging and discharging terms in Eq. (4) represent the change of energy in the storage system over one unit time, i.e. 1 hour as assumed in this study. For conciseness, the time interval of 1 hour is not shown in Eq. (4). It is important to point out that Eq. (4) considers all power deficit to be met by the ESS because a fully renewable operation is assumed. The energy flow around the storage at a particular time t is defined by $L(t+1) - L(t)$, where a positive value indicates charging and a negative value indicates discharging. Since L^{cap} is normalised by the hourly energy consumption, its value also represents the number of production hours that can be powered solely by the ESS.

When the storage system is to be connected to a chemical production process, its conversion efficiency needs to be revised to take the chemical process characteristics into account. Traditionally, the efficiency is assumed to be 0.6 in both charging and discharging of a H_2 -based ESS with a technical nature similar to the one considered in this study [11], which coincides with the round-trip efficiency of 30–40% reported by Beaudin et al. [26]. The overall efficiency takes into account the energy losses from water electrolysis, H_2 compression and energy output from the fuel cells. In this work, the specific energy consumption of electrolyzers, which has already accounted for the energy losses, is taken as 4.5 kWh/Nm³_{H₂} [27]. This is equivalent to 55.7 kWh/kg_{H₂} at the electrolyser outlet conditions, and thus the conversion efficiency is found to be 70.7% based on the theoretical energy requirement of 39.4 kWh/kg_{H₂} [28]. Therefore, η_{ch} is considered as a makeup efficiency set to 0.9 (it only addresses the energy losses in the compression process since the specific energy consumption of electrolyzers has already accounted for the energy losses in the water electrolysis process) so that the overall charging efficiency is approximately 60%. More justifications regarding the makeup efficiency are provided in Section 2.6. In the discharging mode, the stored H_2 can be used as either feedstock ($\eta_{dis} = 1$) or for electricity generation through fuel cells ($\eta_{dis} = 0.6$). The discharge efficiency is set to 0.6 when the stored H_2 is fed to the fuel cells because it results in a round-trip efficiency of 36%, which complies with the literature value [29].

Since the two destinations of the stored H_2 have different efficiency, it is clearly more efficient to prioritise the use of the stored H_2 as feedstock for the MeOH synthesis than its use for electricity generation. Since the synthesis of H_2 feedstock accounts for 89% of the total load, the requirement of H_2 feedstock (in terms of power equivalent) is 0.89 normalised by the load. Therefore, in discharging mode the stored H_2 will first feed the MeOH synthesis as feedstock when $-0.89 \leq P_{\delta}(t) < 0$; if the deficit is larger ($-1 \leq P_{\delta}(t) < -0.89$), the stored H_2 will feed both the MeOH synthesis (as feedstock, $\eta_{dis} = 1$) and the fuel cells (to generate

electricity, $\eta_{dis} = 0.6$). Consequently, Eq. (4) is modified to

$$L(t) = \begin{cases} L(t-1) + \eta_{ch} P_{\delta}(t) & P_{\delta}(t) \geq 0 \\ L(t-1) + P_{\delta}(t) & -f_{ELY}^{SYN} \leq P_{\delta}(t) < 0 \\ L(t-1) - f_{ELY}^{SYN} + \frac{1}{\eta_{dis}} [P_{\delta}(t) + f_{ELY}^{SYN}] & P_{\delta}(t) < f_{ELY}^{SYN} \\ 0 & L(t-1) + \eta_{ch} P_{\delta}(t) \geq 0 \end{cases} \quad (5)$$

where f_{ELY}^{SYN} represents the fraction of load that goes to H_2 feedstock synthesis through electrolysis (which is 0.89 in the MeOH production considered in this work). This parameter is of special interest as it implies how efficient the H_2 -based ESS would be for a chemical production that requires H_2 as feedstock.

2.3.2. The case with dispatchable power

Although the inclusion of a dispatchable power source reduces the management difficulties, this flexibility poses an additional complexity in modelling due to the extra degree of freedom. In Eqs. (4) and (5), the time series of storage profile and its corresponding L^{cap} target a fully renewable operation. In the scenario of a partial renewable operation (due to the use of dispatchable energy), the storage size is not constrained by L^{cap} . Consequently, dispatchable power will be required at time intervals when the VRE and ESS combined output is insufficient. To determine the time series of $L(t)$ in a scenario with dispatchable source backup, the power mismatch needs to be revised by considering the storage capacity as a decision variable (L^{dv}). Note that the revised power mismatch, $P_{\delta}^{re}(t)$, indicates the mismatch between the renewable power system and the load taking the ESS into account, whereas $P_{\delta}(t)$ is the power mismatch between the renewable power generation (excluding the ESS) and the load. The algorithm for the calculation is shown in Algorithm 1 in Appendix A. Also note that $L(t)$ and $P_{\delta}^{re}(t)$ are related in that $L(t)$ determines $P_{\delta}^{re}(t)$ and $P_{\delta}^{re}(t)$ in turn determines $L(t+1)$.

In the analysis, the operation starts and ends with full storage, i.e. $L(t=1) = L(t=8760) = L^{dv}$. The range of L^{dv} is varied from 0 to L^{cap} since L^{cap} is the storage size indicating a fully renewable operation, and thus any value higher than L^{cap} will not reduce the dispatchable energy requirement. Note that the full storage is defined as a positive number, contrasting to 0 in the fully renewable operation. This is because in the fully renewable operation L^{cap} is calculated from the storage profile, whereas L^{dv} in the partial renewable operation is a decision variable that determines the storage profile. Nevertheless, both definitions are equivalent as the energy flow from the ESS at time t , defined by $L(t+1) - L(t)$, is the same.

The energy structure of the load can be derived from the same algorithm as the cumulative dispatchable energy is obtained from the profile of $P_{\delta}^{re}(t)$, and the energy from the ESS is obtained from $L(t)$. The time series of dispatchable power requirement, $P_D(t)$, is calculated by

$$P_D(t) = \begin{cases} |P_{\delta}^{re}(t)| & P_{\delta}^{re}(t) < 0 \\ 0 & P_{\delta}^{re}(t) \geq 0 \end{cases} \quad (6)$$

The dispatchable energy requirement, E_D , is essentially the integration of dispatchable power over the period of analysis divided by the total number of hours. Since the original VRE data are available in an hourly scale, E_D can be approximated by

$$E_D = \frac{1}{N} \sum_{t=1}^N [P_D(t) \times 1] \quad (7)$$

Note that E_D is normalised by the total energy load in a year, which is $8760 \times P_L$ (i.e. 5256GWh). Due to the normalisation, the numerical value of E_D also represents the fraction of load that has been met by dispatchable energy, and $1 - E_D$ indicates the renewable penetration (f_L^{RE}), i.e. the fraction of load met by renewable energy.

The power scheduling is essentially determined from $L(t)$ profiles as all other time series are dependent on $L(t)$. The production is powered from the energy sources that are prioritised as follows: (1) power from renewable generation; (2) H_2 from the ESS as feedstock (which is power

equivalent); (3) power from the ESS via SOFC and (4) power from a dispatchable source (if it is available). This implies that the dispatchable energy cost is higher than that of the renewable power system (including the power generation and the ESS). The cases of lower dispatchable energy prices are discussed in the section of economic analysis. The power scheduling for the fully and partially renewable operation is visualised in Supplementary Fig. S6.

2.3.3. Define start time and status

It is important to note that the $L(t)$ profile depends on both the initial state of storage and the start time of operation in a year. For convenience, a complete cycle of storage operation is defined as full-to-null-to-full (in contrast to null-to-full-to-null). As an illustration, examples of $L(t)$ profiles are plotted with varied γ at fixed f_W over a period of 4-year (see Supplementary Fig. S4). The $L(t)$ profile continues to the next year by repeating the same meteorological data, thus generating perfect cycles of charging and discharging profiles. If true meteorological data of consecutive years were used, the charging/discharging cycle may vary accordingly (and so the value of L^{cap}). There are more discussions in Section 4.1 regarding the use of historical VRE data and its limitations. Nevertheless, the purpose of the plot (Supplementary Fig. S4) is (1) to demonstrate that the start time of operation has to be considered, and (2) to identify the characteristic period of operation, which is equivalent to one year. Consequently, the analysis is performed at the beginning of the characteristic period instead of at the beginning of a calendar year.

2.4. Economic optimisation

The economic potential of the concept is evaluated by the levelised cost of MeOH (LCOMeOH, calculated in \$/tonne), which is defined by

$$LCOMeOH = \frac{1}{M_{MeOH}} \left[\frac{TFCC \cdot r(1+r)^n}{(1+r)^n - 1} + P_L N \cdot LEC + C_{ELY}^{SYN} + \sum_j C_j \right] \quad (8)$$

where TFCC stands for the total fixed capital cost of the MeOH plant (including CO₂ capture and MeOH synthesis but excluding the renewable power generation and its ESS), r represents the discount rate (taken as 8%), n is the life of the plant (assumed to be 30 years), LEC stands for the levelised energy cost (\$/MWh) of the energy delivered from the renewable power system (including power from renewable generation and its ESS) to the MeOH production, C_{ELY}^{SYN} is the annualised cost of the electrolyzers for the MeOH synthesis loop, C_j is the annual cost of utility j (including process water and cooling water) and M_{MeOH} is the total mass of MeOH produced in a year. The material cost of flue gas (source of CO₂) is assumed to be free. Note that all parameters in Eq. (8) are fixed except LEC since the production is operated on a steady-state basis. Therefore, minimising LCOMeOH is equivalent to minimising LEC, which is calculated by

$$LEC = \frac{1}{P_L N} \left[\sum_{i=W,S} \left[\gamma f_i P_L \frac{1}{CF_i} \frac{r(1+r)^n}{(1+r)^n - 1} CapEx_i^{GEN} \right] + \sum_{i=W,S} \left[\gamma f_i P_L \frac{1}{CF_i} OpEx_i^{GEN} \right] + C_{ELY}^{ESS} + \frac{\eta_{ch} L^{dv} P_L}{e_{ELY}} \frac{r(1+r)^n}{(1+r)^n - 1} CapEx^{ST} + c_D E_D P_L N \right] \quad (9)$$

where CF_i stands for the capacity factor of renewable source i , $CapEx_i^{GEN}$ is the capital expenditure per unit power generation capacity for renewable source i , $CapEx^{ST}$ is the storage capital expenditure per unit H₂ capacity (measured in tonne), $OpEx_i^{GEN}$ is the operational expenditure per unit power generation capacity for renewable source i , c_D is the unit price of dispatchable power and e_{ELY} is the specific energy consumption of water electrolysis, which is taken as 55.7 kWh/kgH₂. Unlike the constant annualised electrolyzers cost for the synthesis loop (C_{ELY}^{SYN}), the annualised electrolyzers cost for the ESS (C_{ELY}^{ESS}) is a variable subject to the optimiser, as shown in Eq. (10):

$$C_{ELY}^{ESS} = \frac{r(1+r)^n}{(1+r)^n - 1} CapEx^{ELY} P_{ELY}^{ESS} \quad (10)$$

where $CapEx^{ELY}$ is the electrolyzer capital expenditure and P_{ELY}^{ESS} denotes the rated power of the electrolyzers for the ESS.

For the partially renewable operation, the model aims to minimise LEC with an objective function defined by

$$\begin{aligned} \min. \quad & LEC = f(\gamma, f_W, L^{dv}) \\ \text{s.t.} \quad & 0 \leq \gamma \\ & 0 \leq f_W \leq 1 \\ & 0 \leq L^{dv} \leq L^{cap} \end{aligned} \quad (11)$$

Energy balances outlined in Supplementary Fig. S6

Note that the constraint of γ is loose because all power deficit can be met by dispatchable source if the combined power of renewable generation and its ESS is insufficient. For the fully renewable operation, LEC can be minimised subject to the condition that the production is sustainable without any dispatchable source. This leads to

$$\begin{aligned} \min. \quad & LEC = f(\gamma, f_W) \\ \text{s.t.} \quad & \gamma_{min} \leq \gamma \\ & 0 \leq f_W \leq 1 \end{aligned} \quad (12)$$

Energy balances outlined in Supplementary Fig. S6

The condition of $\gamma_{min} \leq \gamma$ is equivalent to $P_{\delta}^{re}(t) \geq 0$ for all t , which implicitly determines γ_{min} . Note that for a fully renewable operation L^{dv} is equal to L^{cap} in Eq. (9), which is calculated at a given γ (provided that $\gamma \geq \gamma_{min}$) and a given f_W (i.e. L^{cap} is a function of γ and f_W , $\gamma \geq \gamma_{min}$ is a constraint and γ_{min} is a function of location and f_W). The optimisation problems are solved using the *FMINCON* solver in Matlab, which employs a non-linear programming (NLP) method. The default setting of the *FMINCON* solver is used.

The TFCC of the MeOH plant is adopted from our previous work [25], which was scaled via the six-tenths factor rule based on the work of Zhang et al. [30] and updated to 2018 using the annual chemical engineering plant cost index. Detailed TFCC, raw material costs, utility price and renewable power system costs are available in Supplementary Tables S1–S4.

2.5. Renewable energy data

To incorporate renewable energy in chemical production it is often vital to select a suitable location with sufficient VRE availability and necessary infrastructures. Here, the meteorological data of wind and solar sources from two locations (Kramer Junction and Norderney) are used as an example to perform the numerical studies of VRE integration as well as exploring the impact of their characteristics on the storage and balancing synergies.

The solar and wind data are obtained from Meteornorm, a meteorological database that provides hourly data for different locations. The global horizontal radiation (measured in kWh/m²) is used as available solar power with a 15% efficiency. The wind velocity provided in Meteornorm (measured at a height of 10 m) is first converted to a hub height of 80m, which is calculated by Supplementary Eq. (S1). The hub height velocity then inputs to the power profile of a specific turbine to generate wind power. The turbine that has been selected in this study is a Vestas V90 model with a power profile shown in Supplementary Fig. S7. The cut-in and cut-out speeds are set as 4 m/s and 25 m/s, respectively [31].

Since the model of the wind turbines (3.0MW) is selected, the yearly mean power generation per turbine can be calculated according to the wind speed of each location. This gives the CF of wind power to be 4.3% for Kramer Junction and 29.4% for Norderney, respectively. Regarding the solar power, the CF for Kramer Junction is assumed to be 25.0% (this is the CF of solar PV farms used in the work of Matzen et al. [32]), whereas the CF for Norderney is calculated to be 12.1% based on its relative strength to Kramer Junction. As discussed previously, neither a standalone wind nor a solar energy system can provide a continuous supply of energy. Therefore, a combination of complementary energy sources is considered in this work for the purpose of levelling renewable

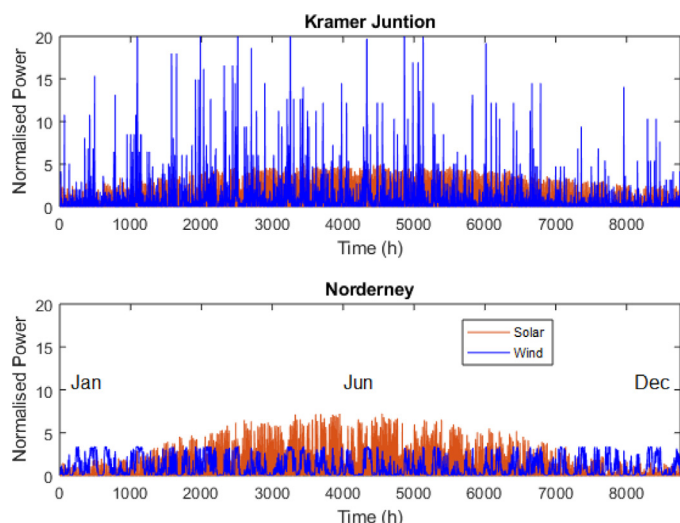


Fig. 3. Year-round availability of wind and solar power of a selected year. (Top) Data obtained from a weather station near Kramer Junction, US; (Bottom) data obtained from Norderney, Germany. Each series is shown in 1-hour resolution and normalised to the respective yearly mean value.

power output, although the wind source in Kramer Junction and the solar source in Norderney are unfavourable.

Fig. 3 depicts the time series of wind and solar power profiles for Kramer Junction (top panel) and Norderney (bottom panel). Note that the data are normalised to the respective yearly mean value, and thus they only reflect the variability of the source but give no information about their strength or availability. Clearly, the two places feature different VRE characteristics, especially in wind energy. The wind power in Kramer Junction varies significantly throughout the year, and it often peaks to as high as 20 times its yearly mean value. In direct contrast, the wind power profile in Norderney has shown remarkable smoothness with the highest variation less than 4 times its mean. The standard deviation (σ) is used to measure the variability of the renewable sources (tabulated in Supplementary Table S6) and finds that the wind power in Norderney is the least variable source. Its consistent power availability is a motivator that drives the wind farm installation in the region. Regarding solar power, both locations show moderate variations in the demonstrated time scale. However, it has a significant fluctuation on the diurnal time scale, which may impede its integration into chemical production or any other power demand that requires a steady input. In addition, solar power has a clear seasonal pattern, which is abundant in the summer and lean in the winter. Since the investigated chemical production has a constant load, the operation would also have a seasonal pattern of power mismatch if solar power dominates the energy supply.

2.6. Summary of assumptions

This section lists the key assumptions in the analysis as well as the justifications: (1) the operation starts at the beginning of the characteristic period of 8,760 hours, which is equivalent to one year. (2) The downtime of production is ignored, which is in line a previous study [33]. (3) The dispatchable source is assumed from the grid with a CO₂ emission calculated according to the generation methods, which is location dependent. (4) The electrolyzers can ramp instantaneously from 0–100% with a constant efficiency [33], which translates to a constant specific energy consumption of 55.7 kWh/kg_{H₂} at the outlet conditions. (5) A separate set of two electrolyzers can be considered in the ESS because (i) the operation of the electrolyzers in the ESS and the MeOH production has concurrent peaks, (ii) the costing is assumed to be linear with respect to size, and (iii) the efficiency of the electrolyzers is assumed to be constant and independent of load. (6) H₂ for the ESS is

stored in steel tanks at a pressure of 172bar, and the standby losses of H₂ in the ESS are ignored [34]. (7) The ESS is not limited by power input or output because additional electrolyzers (for charging) and fuel cells (for discharging) can always be deployed to meet the requirement. (8) The values of η_{ch} and η_{dis} are assumed to be 90% and 60%, respectively. The overall charging efficiency takes the electrolyser efficiency (70.7%) and η_{ch} (this indicates the energy losses during the H₂ compression process) into account. Regarding the discharging side, an efficiency of 60% is assumed for the SOFC [35]. Altogether, the round-trip efficiency amounts to approximately 36%, which is in line with the literature value [29].

3. Results

3.1. Production without ESS

This section investigates the optimal renewable mix and the dispatchable power requirement when the ESS is excluded from the renewable power system. Without an ESS, levelling the power output becomes the key as all surplus power would have to be curtailed. Also, a large amount of dispatchable energy is required because a power deficit is more likely to occur, or alternatively, a large excess generation is required to reduce the likelihood of deficit.

The E_D calculated for Kramer Junction and Norderney are shown in Fig. 4A and B, respectively. Since γ is a measurement of excess generation, the requirement of E_D decreases with increasing γ . Both locations have shown lower E_D at intermediate f_W ; however, their minimum valley pathways vary slightly, which is attributed to the characteristics of their wind/solar availability. It is also interesting to see that the worst scenarios (highest E_D) for Kramer Junction and Norderney lie in opposite f_W . This is ascribed to the different variability of VRE in the two locations, i.e. wind energy is more variable in Kramer Junction, whereas solar energy is more variable in Norderney (see Supplementary Table S6).

The intersecting profiles of Fig. 4A and B at $\gamma = 1.50$ are analysed and plotted with finer granularity in Supplementary Fig. S8. It has been found that the best scenarios (lowest E_D) at $\gamma = 1.50$ for Kramer Junction and Norderney are at $f_W = 0.65$ and $f_W = 0.70$, and their corresponding minimum E_D are 0.41 and 0.30, respectively. Since E_D is normalised by the annual energy requirement at the demand side, this means that the energy for chemical production from the dispatchable source constitutes 41.1% in Kramer Junction or 30.2% in Norderney. This is a significant dispatchable energy requirement even though the average renewable power generation is 1.5 times of the load requirement.

The representative energy mismatch profiles for both locations with $\gamma = 1.50$ at their optimal VRE mix are shown in Fig. 4C and D. The mismatch profile is strongly correlated to the availability profiles illustrated in Fig. 3. Since the average generation of both locations is the same and equals 1.5 times the load requirement ($\gamma = 1.50$), more positive mismatch comes with more negative mismatch so that the total amount of energy is a constant, i.e. Fig. 4C has denser negative mismatch as well as more positive mismatch compared to Fig. 4D. This variability is undesirable and results in an additional management difficulty. As an example, Kramer Junction has shown a much larger dispatchable requirement than Norderney due to its significant variance (since the technology cost function is the same for both locations, the difference in dispatchable requirement is attributed to the variability of renewable sources). The positive mismatch also represents the amount of energy that can potentially be stored. Notice that Fig. 4C and D are plotted on the same scale to reflect the relative variability of the VRE sources at the two locations.

3.2. Production without dispatchable energy source

To power a chemical production with only renewable power can be challenging but it is of significance for production located in an islanded

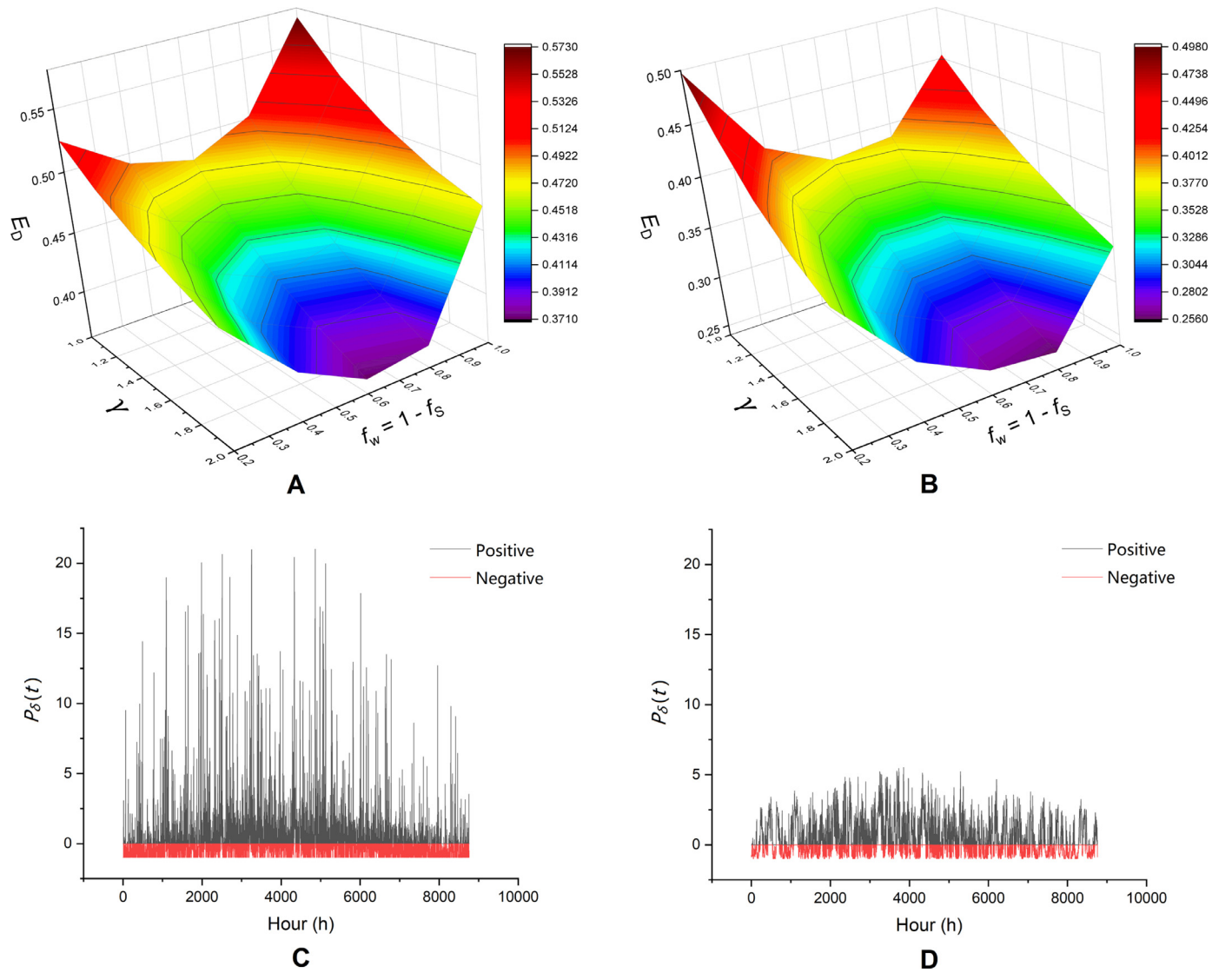


Fig. 4. Top: Requirement of dispatchable energy E_D as a function of γ and the share of wind power f_W at the demand side for (A) Kramer Junction and (B) Norderney. Bottom: Time series of power mismatch in best scenarios when $\gamma = 1.50$, (C) Kramer Junction with best scenario at $f_W = 0.65$; (D) Norderney with best scenario at $f_W = 0.70$. Positive values indicate power surplus that has been curtailed and negative values indicate power deficit. The unit of $P_\delta(t)$ and γ is given in load requirement (MW) at the demand side whereas E_D is normalised by the total annual energy requirement (MWh).

or remote area. This section intends to report the minimum storage capacity (L^{cap}) that permits the fully renewable operation and how its corresponding optimal renewable mix varies with increasing renewable power generation.

The dependence of L^{cap} on f_W and γ is demonstrated in Fig. 5A and B for the MeOH production located in Kramer Junction and Norderney, respectively. The optimal f_W (the f_W resulting in the minimum L^{cap}) at the corresponding γ forms a minimum valley along the contour lines, which is indicated by the dashed line with white markers. In Kramer Junction, the optimal f_W varies significantly from 71% at $\gamma = 1.09$ to 30% at $\gamma = 1.45$. In contrast, the minimum valley of f_W in Norderney varies in a narrow range of 82–96%. This may be attributed to the convexity of the contour lines in Norderney: variation in f_W significantly influences the value of L^{cap} at a given γ . Thus, the optimal mix becomes more deterministic and lies in a narrow range. The shape of contour lines in Kramer Junction is rather flat, meaning that a wide range of f_W would result in a similar L^{cap} provided that γ is unchanged. In summary, L^{cap} is mainly determined by γ in Kramer Junction, whereas it is mainly determined by renewable mix in Norderney.

The sensitivity of L^{cap} to f_W is also shown in Fig. 5C and D where L^{cap} cuts through selected f_W are plotted. The optimal (minimum) L^{cap} is indicated by the dashed line with white markers and the value of the corresponding f_W is shown on the respective contour plots. In Kramer Junction, all ranges of f_W result in a L^{cap} that is close to the optimal L^{cap} (at a given γ). On the contrary, the lines of L^{cap} cuts in Norderney vary dramatically when a different renewable mix is used. Nevertheless, both locations have shown a L^{cap} cut at a particular f_W that is close to the optimal L^{cap} cut at all γ . The value of such a f_W is approximately 50% in Kramer Junction and 75% in Norderney. These plots demonstrate that although the optimal f_W is specific to each L^{cap} and may vary significantly when γ is varied, there may exist a single value of f_W that would result in a L^{cap} close to the optimum at the whole range of γ . This particular f_W is of importance when a power system needs to tackle a demand with variable load (variation from the demand side). In our case study, although the load of chemical production is constant, such flexibility is desirable to tackle the variation from the generation side since the calculation of L^{cap} is based on past data. For instance, the wind and solar harvesting plants designed with an optimal f_W for a given γ

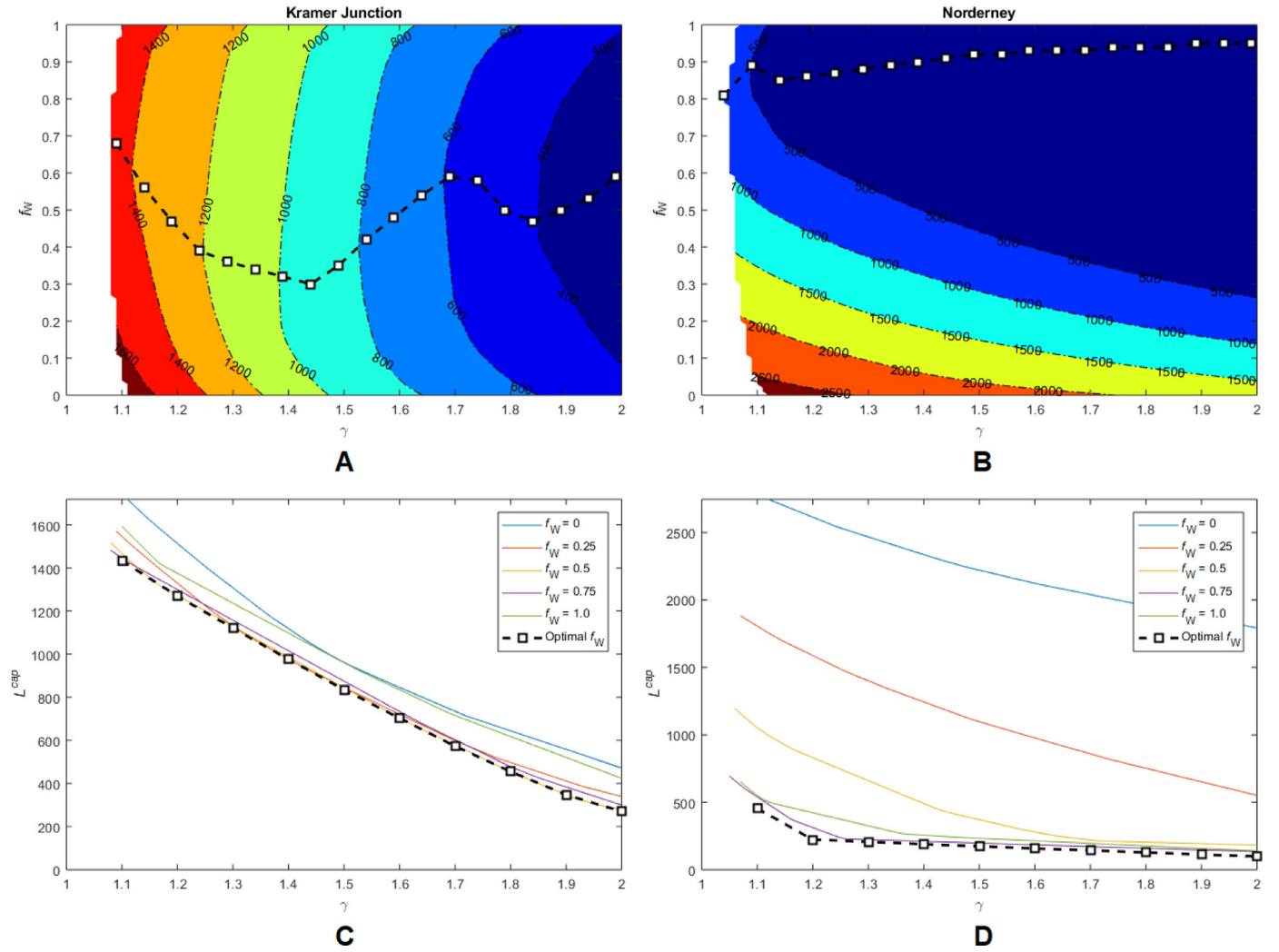


Fig. 5. L^{cap} as a function of f_W and γ for MeOH production without dispatchable source. Top panel: contour plots of L^{cap} for production located in (A) Kramer Junction and (B) Norderney. Bottom panel: L^{cap} cuts through selected f_W for (C) Kramer Junction and (D) Norderney.

in a historical year may encounter a different γ in real-time operation due to the inconsistency in yearly renewable energy availability.

From Fig. 5C it is also observed that L^{cap} decreases significantly and almost linearly with the increase of γ in Kramer Junction. In contrast, L^{cap} in Norderney (Fig. 5D) varies in a narrow range from approximately 500 to 100 when γ is increased from 1.10 to 2.00. In particular, when $\gamma > 1.20$ the value of L^{cap} is almost independent of γ . This is attributed to the consistent availability of VRE in Norderney: the maximum power mismatch is only around 5 times the load in the entire year, contrasting with 20 times the load in Kramer Junction (c.f. Fig. 4C and D). This characteristic of the VRE sources greatly eases the management and reduces the cost of running a renewable energy system.

Notice that in Fig. 5A and B there is empty space when γ lies between 1.00 to approximately 1.10. This is because the generation is not sufficient to power the chemical production solely with VRE and its storage (i.e. $\gamma < \gamma_{\min}$). If the energy conversion and storage scheduling were perfect, the generation may be able to meet the load at $\gamma = 1.00$. In our analysis, the operation is tenable only if γ is above 1.10. This is a remarkably small excess generation as compared to the results from Budischak et al. [14], in which they have reported a system that generates 180% (equivalent to $\gamma = 1.80$) of the electrical energy needed by the load when 90% of hours are covered by VRE or 290% ($\gamma = 2.90$) of need when 99.9% of hours are covered by VRE. At an extreme renewable mix (very large or

very small f_W), it is more likely to have insufficient generation (larger γ_{\min} required), which indicates the importance of introducing complementary renewable sources in the fully renewable operation.

Benefited by the chemical process (taking stored H_2 as a feedstock instead of feeding to fuel cells), the storage system is highly energy-efficient and is able to provide sufficient power even at small γ . However, the $L(t)$ profile (and its corresponding L^{cap}) depends on both energy efficiency and γ . Operations at small γ may incur a significant increase in L^{cap} , thus increasing the cost of ESS. To demonstrate the impact of γ on $L(t)$ and L^{cap} , profiles at selected γ are plotted for Kramer Junction (Fig. 6A) and Norderney (Fig. 6B) over its characteristic period of operation, starting from full storage and ending in a fully charged status. For clarity, the $L(t)$ profiles are converted from energy term normalised by the load to its equivalent H_2 mass in tonne on the basis of a 600MW MeOH plant. A unique difference of the profiles between the two locations is the dependence of L^{cap} on γ . As suggested in Fig. 5C and D, L^{cap} in Kramer Junction is linearly dependent on γ while L^{cap} in Norderney is relatively insensitive to γ when $\gamma > 1.20$. Similarly, the $L(t)$ profiles for Norderney at $\gamma = 1.55$ and 2.00 almost superimpose onto each other (Fig. 6B). Another noticeable fact is that L^{cap} for Norderney is smaller than that for Kramer Junction in the whole range of γ , indicating much easier management of the power system.

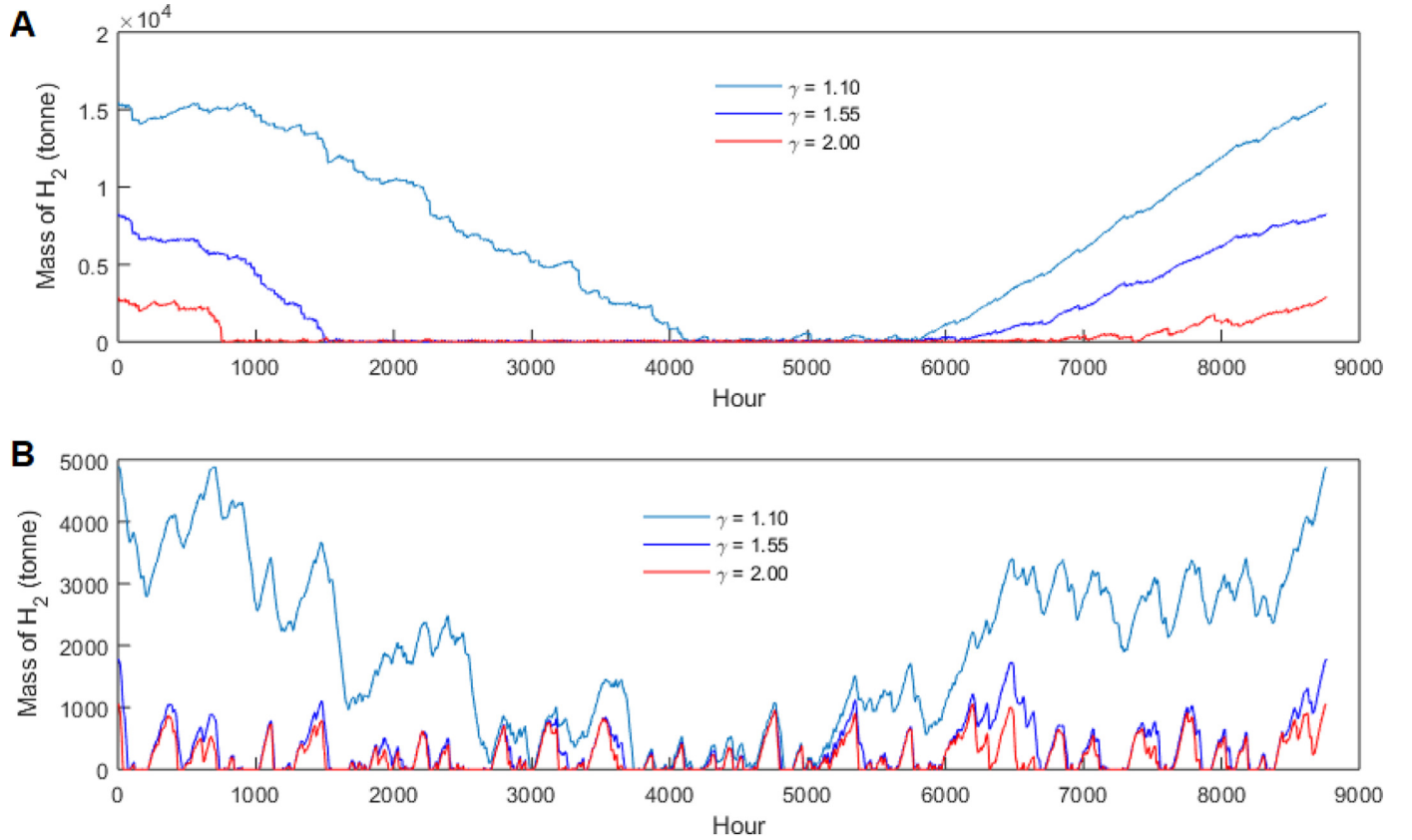


Fig. 6. Time series of $L(t)$ in terms of H_2 mass with optimised L^{cap} at selected γ for a 600 MW MeOH production process located in (A) Kramer Junction and (B) Norderney.

Table 1
 L^{cap} and empty hours of the storage system in Kramer Junction and Norderney.

	Kramer Junction			Norderney		
γ	1.10	1.55	2.00	1.10	1.55	2.00
L^{cap} (tonne of H_2)	15,438	8,279	2,909	4,889	1,788	1,063
empty hours (%)	1.0	15.8	24.2	2.9	21.9	31.8

The value of L^{cap} and the fraction of empty hours at different γ for both locations are summarised in Table 1. It is found that the number of empty hours increases with increasing γ for both locations. This is expected as the system is less likely to encounter a power deficit when the generation is excess. By analysing the profile of $L(t)$, the empty hours are found concentrated in a certain period of operation for both locations when γ is small, implying a strong seasonal pattern. However, at higher γ the $L(t)$ profiles for Norderney are not seasonally dependent as the empty hours spread throughout the period of operation. On the other hand, Kramer Junction has demonstrated a reduced seasonal dependency at higher γ . The implication that may be drawn from the analysis is that a large quantity of seasonal storage is essential for operation in Kramer Junction, whereas a small but more efficient short-term storage may be used in Norderney to reduce the cost. The underlying reason may be the fact that the wind power dominates in Norderney (optimal f_W ranges from 88–95%), which is not seasonally dependent, whereas solar and wind power play an equal role in Kramer Junction (optimal f_W ranges from 43–65%), wherein solar power has a strong seasonal pattern. It is noteworthy that the $L(t)$ profile for Norderney at $\gamma = 1.10$ is affected by both the seasonal and short-term (e.g. weekly scale, contrasting to diurnal scale) variation as the optimal mix is determined to be $f_W = 88\%$, wherein solar power has an increased share in the generation.

3.3. Production powered by a mix of VRE and dispatchable energy

To meet a load solely by renewable power poses a stringent constraint on the system design. In the aforementioned example, Budischak et al. have reported an 80% increase in the renewable power generation to increase the hours of grid operation covered by all renewables from 90% to 99.9% in the cost-minimised case [14]. In this work, to power the chemical plant solely by renewables requires either large excess generation or significant VRE storage capacity. The immediate question is how much we are willing to pay for a fully renewable system. To answer the question, it is important to explore the marginal benefit if a small fraction of the load can be met by dispatchable energy. This can be approached by demonstrating the dispatchable energy requirement with different storage size ranging from 0 to L^{cap} . Note that the storage size at 0 and L^{cap} are two special cases, which respectively represent an operation without storage and an operation without dispatchable energy (i.e. fully renewable).

The correlation between dispatchable energy requirement and storage size is illustrated in Fig. 7. From the insets of Fig. 7 it can be seen that both locations demonstrate a highly concave E_D with respect to the increase of L^{dv} , leading to two regimes of different behaviour. At the outset, a small introduction of storage dramatically reduces E_D whereas the reduction levels off at subsequent increases of the storage capacity. The threshold L^{dv} lies in the range of 16–18. Since L^{dv} is normalised by the hourly energy requirement, its value also indicates the number of production hours that can be solely powered by the storage starting from full to null. For simplicity, Fig. 7 is plotted with constant f_W (50% for Kramer Junction and 75% for Norderney) for all γ . This is because at the selected f_W the result is very close to the optimum (c.f. Fig. 5C and D).

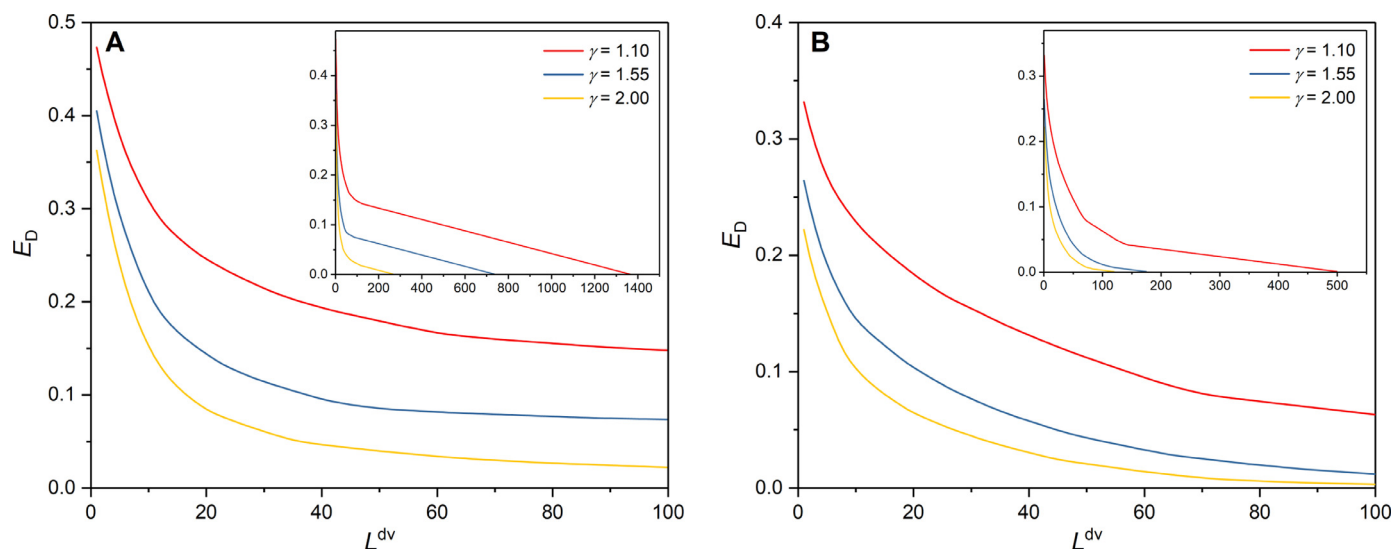


Fig. 7. Dispatchable energy requirement E_D as a function of L^{dv} varied in a small range. The insets show full range of L^{dv} up to L^{cap} . E_D is normalised by total annual energy requirement ($8760 \times P_L$) while L^{dv} is normalised by hourly energy requirement. (A) for Kramer Junction (f_w is fixed at 50% for all γ) and (B) for Norderney (f_w is fixed at 75% for all γ).

The two regimes of different behaviour in Fig. 7 may be ascribed to the diurnal pattern of the solar power as it is only abundant during the midday (6 h) and it is more likely to encounter an energy deficit in the rest of the day (18 h). Therefore, a small introduction of storage becomes vital to the intraday operation, which stores positive $P_o(t)$ during the daytime and meets negative $P_o(t)$ during the night. As a comparison, the relation between storage capacity and dispatchable energy requirement is plotted at $f_W = 0.01$ and $f_W = 0.99$ in Supplementary Fig. S10. Clearly, the concavity of the plot is reduced at a high wind fraction. In contrast, a sharp change is observed at a high solar fraction, indicating the significant impact of intraday storage on the operation when solar power dominates the generation.

Since the marginal benefit (reduced E_D) decreases dramatically when L^{dv} is above 18, it may not be economically attractive to achieve a higher renewable penetration. Significantly, at $L^{\text{dv}} = 18$, the renewable penetration is already as high as 84.7% in Kramer Junction and 88.9% in Norderney at an intermediate excess generation ($\gamma = 1.55$). To further increase the renewable penetration up to 99%, it would require a L^{dv} to increase by 36.6 times ($L^{\text{dv}} = 659$) for Kramer Junction and 6.1 times ($L^{\text{dv}} = 110$) for Norderney, respectively. Since the intraday variation can be effectively managed by a storage size of 18, the significant increase in storage size for a 99% renewable penetration operation is attributed to the synoptic and seasonal variation of the renewable sources (particularly in the case of Kramer Junction, in which the solar source dominates the renewable power generation).

3.4. Economic analysis

The economic potential of the MeOH production is mainly determined by the LEC that is optimised by γ , f_W and L^{dv} (or L^{cap} if the objective function aims at a fully renewable operation). To take renewable harvesting plants into economic consideration is challenging not only because of the influence of policy on the price of electricity generated from VRE but also due to the fast development of renewable technologies. Here, benchmark prices of the inland wind farm, photovoltaic (PV) farm and H_2 -based ESS are used to report the true economic potential by excluding the subsidies and renewable incentives.

In the scenario of a partial renewable operation, a benchmark price of dispatchable energy is assumed to be 230\$/MWh, which is the EU average electricity price in 2017 [36]. Table 2 summarises the optimal LEC (see Eq. 9, in which the results are obtained from the *FMINCON*

Table 2

LEC optimised by excess power generation, renewable mix and storage capacity for production powered by both VRE and dispatchable sources.

	LEC (\$/MWh)	γ	f_W	L^{dv}
Kramer Junction	105.6	1.07	0	20
Norderney	103.1	1.12	0.91	130

NLP solver) and its corresponding γ , f_w and L^{dv} . The LEC for Kramer Junction and Norderney is found to be 106\$/MWh and 103\$/MWh, respectively, which are close to each other. However, the renewable penetration in the optimal design is much higher in Norderney ($f_L^{\text{RE}} = 96.0\%$) than in Kramer Junction ($f_L^{\text{RE}} = 81.2\%$) at a (albeit slightly) lower LEC. This implies that although the two locations have the similar economic performance at the chosen dispatchable energy price, the environmental performance is better in Norderney. Since more renewable energy is used in Norderney, the size of EES is expected to be larger. Indeed, the required storage capacity in Norderney is found to be 130 (normalised by the hourly load), which is 6.5 times higher than the one in Kramer Junction. Regarding the renewable source in power generation, Norderney shows a renewable mix of 91% wind and 9% solar power in the generation, whereas Kramer Junction uses a sole power source (i.e. solar energy). Although the complementarity of renewable sources can mitigate the variability in power generation (thus reducing storage cost), the wind source in Kramer Junction is too costly to be integrated (CF of wind Kramer Junction is as allow as 4.3%). The corresponding LCOMeOH for Kramer Junction and Norderney at the optimum is found to be 1490\$/tonne and 1459\$/tonne, respectively.

The dispatchable power is usually (but not necessarily) the electricity from the grid, and its price varies significantly by region. The optimised LEC (and its corresponding γ , f_w and L^{dv}) is highly dependent on the dispatchable power: when the dispatchable power is expensive, the implementation of renewable power is justified economically; when the dispatchable power is cheap, the chemical production may simply run on dispatchable power without any renewable energy. Therefore, it is of importance to report the correlation between dispatchable energy price, the optimal LEC and their corresponding renewable penetration. Fig. 8A shows the economic performance measured in LEC. Significantly, Kramer Junction has better economics than Norderney

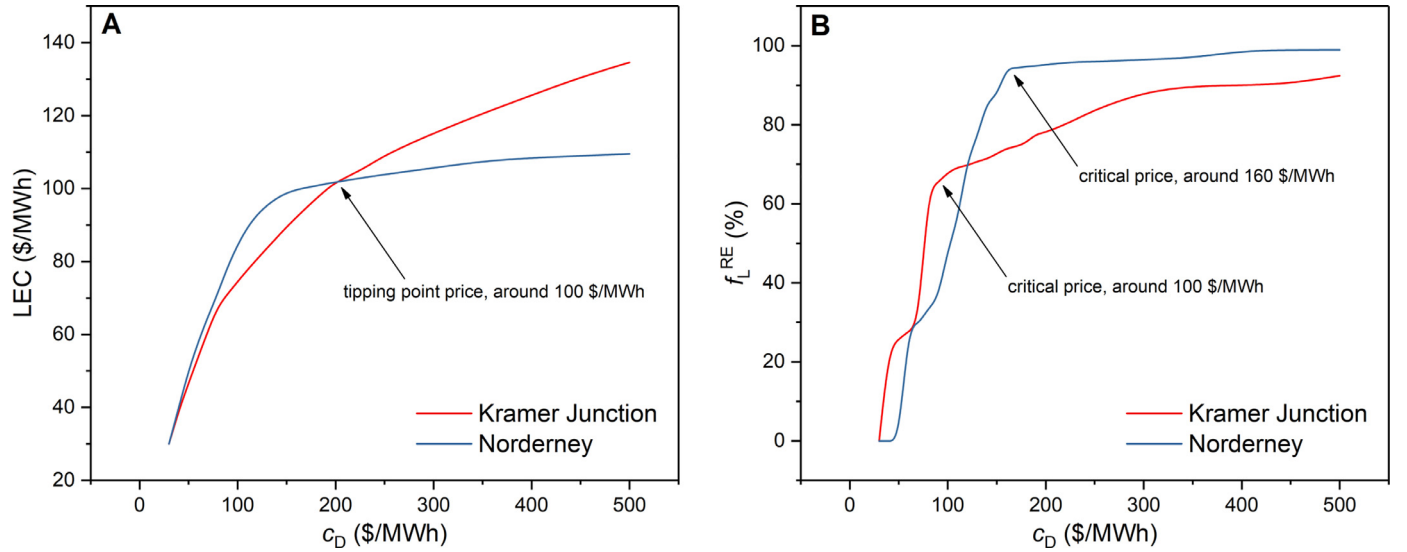


Fig. 8. The impact of dispatchable energy price on (A) LEC and (B) renewable penetration.

Table 3

LEC optimised by excess power generation, renewable mix and storage capacity for production powered by VRE and its ESS only.

	LEC (\$/MWh)	γ	f_w	L^{cap}
Kramer Junction	166.8	1.89	0.00	467
Norderney	114.0	1.16	0.86	252

at cheaper dispatchable energy prices; however, the opposite can be seen when the price is above 200\$/MWh. Furthermore, the value of LEC in Norderney becomes insensitive to the increase of dispatchable energy price when it is above approximately 150\$/MWh, contrasting to the trend in Kramer Junction. Regarding the renewable penetration (which is a result of the optimal operation), there exists a threshold dispatchable energy price, below which no renewable energy would be implemented (due to higher costs). This threshold price is approximately 40\$/MWh and 60\$/MWh for Kramer Junction and Norderney, respectively. More importantly, the resulting renewable penetration for both locations has a two-regime behaviour: when dispatchable energy is below the critical price, the renewable penetration (in the most economical scenario) increases dramatically with the increase of dispatchable energy price. Above the critical price, the renewable penetration levels off (see Fig. 8B). This two-regime behaviour suggests that the dispatchable energy price may be used as a tool to predict and influence the renewable penetration in a specific end-user [37]. In general, the increase of dispatchable energy prices would encourage the implementation of renewable energy. However, when it is increased higher than the critical price, the marginal benefit is decreased. Notice that the renewable penetration does not increase smoothly because the optimum is determined by both the renewable power generation and the storage capacity. Therefore, it can only be determined empirically as a function of the synergy between renewable source quality, storage costs and dispatchable energy price.

In the case of an islanded operation where dispatchable power is not available, the chemical production has to rely solely on VRE and its ESS. The optimised LEC without dispatchable power for both locations are tabulated in Table 3. At the optimum, excess generation is required at a higher level in Kramer Junction than in Norderney, as opposed to the results in Table 2. This is attributed to the highly variable solar energy in Kramer Junction, which requires excess generation to fulfil the load. Consequently, the required storage capacity also increases accordingly. Although the optimal LEC is increased for both lo-

cations for the fully renewable operation, the cost in Norderney only increases to 1.1 times the original value. In contrast, the cost in Kramer Junction increases by 1.6 times. It is also interesting to see that the optimised LEC for Norderney is obtained when an increased share of the complementary renewable source (i.e. solar energy) is introduced. This is because the balancing becomes more challenging (which is mitigated by the complementarity of renewable sources) when backup dispatchable power is not available. If the objective function focuses on the storage sizing (i.e. focusing on the balancing instead of economics), the renewable mix would be more important (see Fig. 5). Note that the optimal LEC for a fully renewable operation also represents the ultimate LEC in Fig. 8A when the dispatchable energy price approaches infinite.

The LCOMeOH for Kramer Junction and Norderney with 100% renewable energy is increased to 2250\$/tonne and 1595\$/tonne, respectively. In a recent work, Bos et al. reported an analysis of wind-powered MeOH production with a cost of 800€/tonne (or 938\$/tonne) [20]. However, the authors ignored the variability of the renewable source when integrated into the MeOH production, which is a major cost driver. Gonzalez-Garay et al. also reported a range of production cost for wind- (approximately 1,400–1800\$/tonne) and solar-powered (2,300–2400\$/tonne) MeOH [19]. Tountas et al. reviewed the solar-assisted MeOH production thoroughly and analysed the economic performance however using a simplified method [38]. In their report, the minimum selling price for the solar-powered MeOH through PV-electrochemical is 5800\$/tonne. All of the above work circumvented the challenge of renewable source variability by using either a fixed energy cost [20], fixed H_2 price [19] or fixed production cost [38]. This current work complemented the gap by taking the renewable characteristics into account, in which the variability and intermittency are addressed by the ESS and production process itself.

The energy structure of the load in the most economical and fully renewable scenarios for both locations is plotted in Fig. 9. In the fully renewable operation, the dispatchable energy (E_D) for both locations is eliminated by an increased share of the energy from the storage unit (E_{ST}). Note that for Kramer Junction the share of the energy from direct renewable generation (E_G) only increases by a small fraction (from 42% to 45%) even though γ is significantly increased (from 1.07 to 1.89), meaning that a significant portion of renewable energy is curtailed (voluntarily) due to its variability. A sample of energy flow, which is composed of E_D , E_{ST} and E_G , is plotted over a period of one week for both locations in Supplementary Fig. S11.

Although the fully renewable operation is more costly than the most economical operation (i.e. with dispatchable power backup), its signifi-

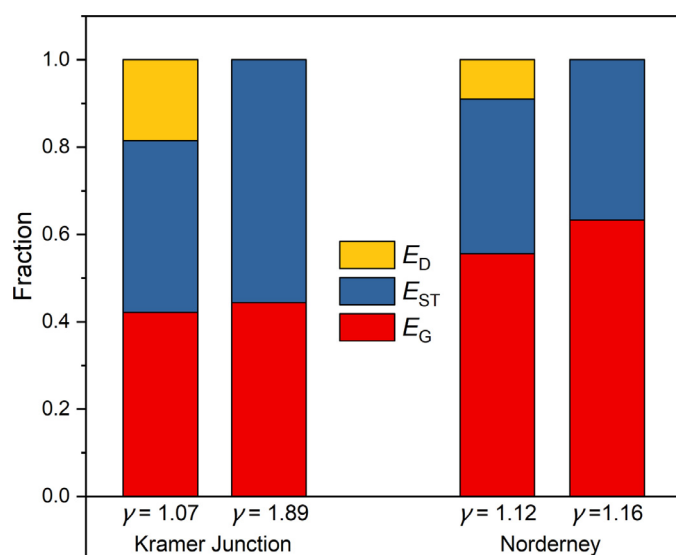


Fig. 9. Energy structure of the load at the most economical scenarios with (left of the group) and fully renewable scenarios (right of the group). E_D denotes the energy from dispatchable power, E_{ST} denotes the renewable energy that goes through the ESS, E_G denotes the energy directly from the renewable power generation.

Table 4

CO₂ emissions for different operation scenarios. Negative value indicates CO₂ avoidance. The CO₂ emission from traditional MeOH process is obtained from Ref. [43].

Scenario	Location	CO ₂ from E_D (kg/kWh)	CO ₂ emissions (kg/kg _{MeOH})
Traditional	–	–	2.97
Fully renewable	–	–	–1.35
Most economical	Kramer Junction	0.69	0.21
	Norderney	0.49	–0.77

cance lies in industrial decarbonisation. For the MeOH production in this work, the fully renewable energy operation would result in a CO₂ avoidance (due to consumption of CO₂ in MeOH synthesis) of 1.35 kg/kg_{MeOH} (obtained from carbon balance), whereas the most economical operation (at c_D = 230 \$/MWh) would have a CO₂ avoidance of 0.77 kg/kg_{MeOH} for Norderney (CO₂ emission from dispatchable energy is assumed to be 0.49 kg/kWh based on the German power generation industry [39]), and would result in a CO₂ emission of 0.21 kg/kg_{MeOH} for Kramer Junction (CO₂ emission from dispatchable energy is calculated to be 0.69 kg/kWh based on the data from the US Energy Information Administration [40]). The CO₂ emissions for all operation scenarios are tabulated in Table 4 and compared with a traditional MeOH production using coal as feedstock. Clearly, the electrified MeOH production significantly reduces the CO₂ emissions even in a partially renewable operation. Although such a concept is not currently economically justified, with advances in renewable technologies and enforced environmental policies, its economic performance will enhance particularly in regions with abundant renewable sources. As an example, the cost of solar PV has decreased dramatically—faster than any previous predictions [41]. This will greatly improve the economics of renewable chemical production since the renewable power generation costs account for a significant portion of the total production cost [42].

3.5. Sensitivity analysis

Due to the fast development in renewable technologies as well as policy incentives, costs reduction in renewable implementation may continue to be foreseen in the near future. Consequently, an economic anal-

ysis based on the current costs is not adequate. The uncertainties in selected key cost variables are thus investigated through a sensitivity analysis. Note that the sensitivity test focuses on the cases with ESS and dispatchable energy backup because they are more likely to be implemented, contrasting to the fully renewable operation that is less economically feasible. The parameters for 0% variation, i.e. the base case in the sensitivity test, are tabulated in Supplementary Table S5. Here, LCOMeOH is reported in the sensitivity analysis because the CapEx of the electrolyzers in the MeOH plant is also considered.

As illustrated in Fig. 10, the LCOMeOH for the two different locations behaves differently with respect to the change of the selected variables. However, both locations are highly sensitive to CF, which is an indicator of the quality of renewable sources. Moreover, the OpEx of renewable power and H₂ storage cost have a negligible impact on the LCOMeOH in both locations. A unique difference between the two locations is the influence of dispatchable energy price: the LCOMeOH in Kramer Junction is highly dependent on the dispatchable energy price, whereas its impact is insignificant in Norderney. This is attributed to the high renewable penetration in Norderney, which reduces its reliance on dispatchable power. Note that only solar power is considered for Kramer Junction and only wind power for Norderney as the most economical scenario results in no (or very little) inclusion of the complementary renewable source. Also note that there are some non-linear behaviours observed in the sensitivity test. This is attributed to the interplay between variables. For instance, when CF is varied, the renewable penetration at the optimum will also vary accordingly, leading to new optimal storage capacity and LCOMeOH.

4. Discussion

4.1. Limitations

A significant limitation in the analysis is the use of historical meteorological data, which limits its use for future implementation. For instance, an optimised ESS for a chemical plant for a particular year may not be sustainable if the year of actual implementation has less abundant renewable energy, or alternatively, it may be over-designed (thus not optimised) if the renewable energy is more abundant than usual. A popular method to generalise the analysis based on non-deterministic variables is to adopt a random-input simulation using probability distributions [44]. However, the theoretical distribution is often based on historical data, and thus its improvement shall be questioned. It would be more helpful to use predicted meteorological data so that the designed renewable power system would be more reliable in a future scenario. Nevertheless, the seasonal behaviour of the VRE in a particular location by-and-large remains the same. Although the time series of energy flow may be different at a specific point, both diurnal and seasonal variations are relatively predictable. Therefore, the analysis based on historical data is able to provide an indicative result. Most importantly, the results of sensitivity analysis and the correlation between renewable quality and storage capacity can provide important insights for policy-making.

Another related limitation is the use of the meteorological data obtained from a specific location. The two case study locations, i.e. Kramer Junction and Norderney, are selected because they are traditionally a good spot for solar and wind energy harvesting, respectively. For instance, Luz International has developed a series of solar electricity generating systems at Kramer Junction in the 1980s to 1990s [45], and Norderney is known for its large offshore wind farm installation. The calculated CF value for wind power in Norderney (29.4%) also justifies the choice of the location since a typical CF of renewable power generators ranges from 20% to 40% [46]. However, the study focusing on a specific location lacks generalisation. Currently, it is challenging to provide a generalised framework using a typical location as a case study. On the other hand, the gap can be complemented by performing a global analysis. Such an analysis has recently been performed by Nayak–Luke

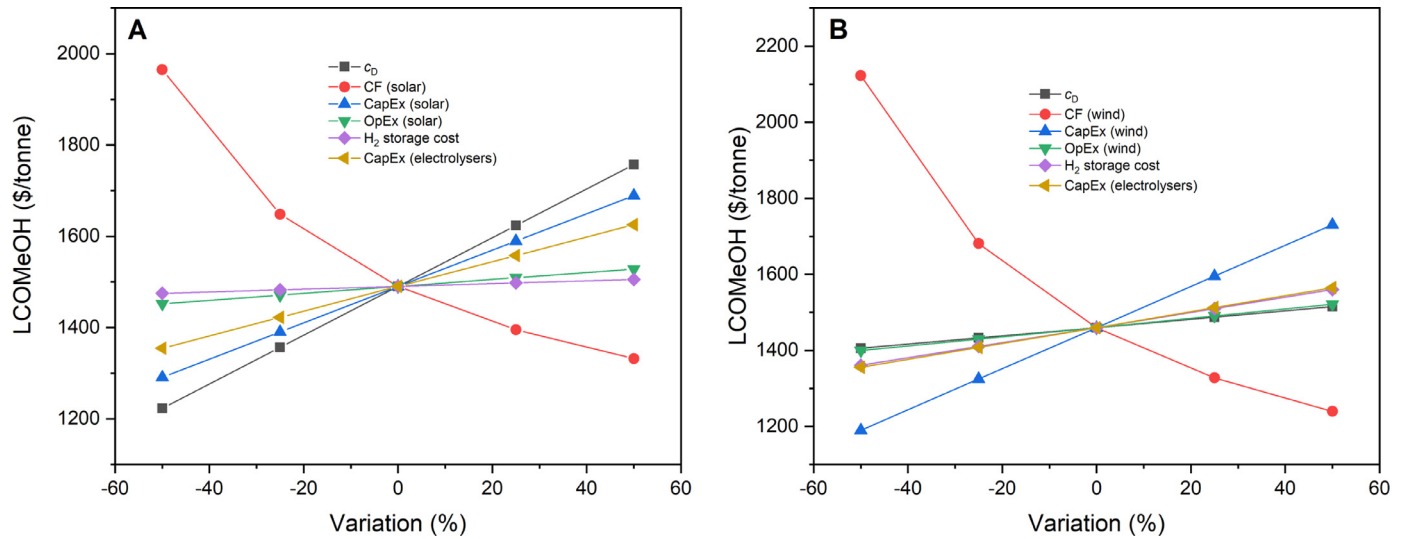


Fig. 10. Sensitivity analysis: (A) Kramer Junction and (B) Norderney.

and Bañares-Alcántara for renewable ammonia production [47], a similar analysis should also be performed for renewable MeOH in the global context.

In this work, we have used a constant dispatchable energy price of 230\$/MWh for the optimisation. However, the actual energy price is highly variable and location dependent. To complement this limitation, the optimal LEC and its corresponding renewable penetration are reported using a range of dispatchable energy price for both locations (see Fig. 8). If the dispatchable source is assumed to be the electricity from the grid, a more accurate analysis could be performed by using a profile of electricity price at an hourly scale.

4.2. Significance of the optimum

The analysis considers two different objectives, i.e. (1) identify the minimum storage capacity for a fully renewable operation, which is a function of f_w and γ ; and (2) minimisation of LEC for both scenarios of fully and partially renewable operation. Many researchers believe that hybrid renewable power systems are usually more reliable and less costly than single-source systems [48]. However, in this economic assessment, the best scenario results in a single renewable source for Kramer Junction and very little complementary source for Norderney. Complementary renewable sources would become vital in certain scenarios, such as (1) relatively equal CF and similar cost for generating power from the additional sources; (2) motivated the implementation of the renewable ESS, i.e. operations in islanded and remote areas or much cheaper storage costs than the generation costs. In summary, the renewable mix in the most economical scenario is often determined by the synergies of the renewable source quality, cost of technologies and operation priority (e.g. reliability, sustainability and economic feasibility) set by the users. Under the current energy market and the cost of renewable technologies, renewable quality dominates the economic potential. This explains why the most economical scenario is composed of only solar for Kramer Junction in the power generation.

It is also important to report the sensitivity of the optimum to the change of variables. For instance, in the optimisation of storage capacity, the optimal L^{cap} in Norderney is extremely sensitive to the change of f_w but not sensitive to the change of γ . The optimal L^{cap} in Kramer Junction has the opposite sensitivity to the same variables. This provides insights into how the optimum responds to the change of variables, and also allows certain flexibility in design if the optimum becomes insensitive.

In the optimisation of LEC for the fully renewable operation, a local optimum has been found, which is close to the global optimal LEC.

This is because a minimum LEC can be achieved at either a small γ with a large L^{dv} or a large γ with a small L^{dv} . It is envisioned that the inclusion of additional decision variables will lead to a non-convex problem, which gives similar results at different combinations of the variable values. Although the results (LEC) are similar, a different value of the decision variables implies a different operation scenario. For instance, a small γ coupled with a large L^{dv} and a large γ coupled with a small L^{dv} lead to a similar LEC but the latter has a much higher renewable curtailment.

4.3. Methods generalisation

As mentioned earlier, using VRE to meet a constant load does not necessarily reduce the complexity in management. In the demonstrated analysis, the chemical process with a constant load is met by two renewable sources. The same method can be applied to variable loads with multiple renewable sources by modifying Eq. (3) to

$$P_{\delta}(t) = \gamma \left(\sum_i f_i \frac{P_i(t)}{\bar{P}_L} \right) - \frac{P_L(t)}{\bar{P}_L} \quad (13)$$

where the subscript i denotes the different renewable sources, $P_L(t)$ denotes variable loads as a function of time and \bar{P}_L is the average load of the period of interest. The management difficulty can be predicted from the profiles of the renewable power and the load. It is desirable to have counterbalanced profiles to reduce the required ESS capacity. The implementation of time-invariant renewable sources, such as geothermal power, can provide a base power generation, thus reducing the overall power mismatch.

4.4. Implications to policymaking

The implications to policymakers are clear: (1) chemical production is not preferred in islanded areas where no dispatchable energy is available; (2) dispatchable energy price can be used as a tool to influence or predict renewable penetration from the economic perspective; (3) economic incentives or penalties such as carbon tax should be implemented to facilitate industrial decarbonisation since the current market does not favour a highly renewable operation; (4) renewable mix is more important when storage becomes vital, e.g. in the case of islanded operation when there is no dispatchable power or when renewable generation is relatively expensive. Under the current market conditions, the complementary renewable source is less important and investment shall go to the harvesting of the energy source that is of the best quality.

4.5. Outlook

The significance of this work lies in the improvement of system efficiency owing to the interplay between chemical processes and the ESS. For a fully renewable operation, the γ_{\min} is as low as 1.10 (c.f. Fig. 5, meaning that the average generation could be only 10% larger than the load requirement provided that the ESS capacity is sufficient). Furthermore, the most economical scenario in Norderney has reported a renewable penetration of 96% while the average generation is only 1.12 times the load (c.f. Table 2), translating to an overall efficiency of 88% for the renewable power system (from renewable power generation outlet to MeOH production inlet). If the same analysis were performed for general energy purposes, the overall efficiency would be much lower.

As a next step, the process of MeOH production can be further investigated as a functional handle for optimisation: in addition to using H_2 as an intermediate energy carrier, raw MeOH product (before distillation process) can be produced as a material buffer using surplus VRE. Thus, the intermittency of VRE would be addressed by both H_2 storage and the intermediate raw MeOH product. The modular operation of a chemical process with excess storage of intermediate products allows DSM for energy scheduling and simultaneously remains steady-state operation for the individual operation unit (except the MeOH synthesis reactor). The separation of the catalytic reaction (to produce raw MeOH) and distillation process (to produce refined MeOH) also provides additional flexibility to better suit the variable nature of renewable sources. A similar concept has been touched on by Hank et al. using a novel dynamic system [49]. However, the work approached the problem using a scenario-based method along with the specified parameters. Given that there has been much interest in the mechanistic insights of how a unit size impacts the overall production process, optimised power scheduling and capacity planning using a modelling approach is highly desirable.

Since the overall efficiency of the renewable use is remarkably high (e.g. γ is 1.16 for a fully renewable operation in Norderney, which translates to an overall efficiency of 86%), refined MeOH may be considered as a competing energy vector to H_2 -based ESS, rather than a commodity. Similar concepts have been proposed by Bñares-Alcántara et al. [50] and Wang et al. [29] using ammonia-based ESS to replace H_2 as an energy vector. With the developments in direct MeOH fuel cells [51], the same concept can be applied to MeOH with advantages of facile management and handling.

5. Conclusions

This work explores a fully electrified MeOH production powered by VRE. The meteorological data of two locations of either good solar (Kramer Junction) or wind (Norderney) resources have been used to investigate the feasibility of renewable MeOH production and the impact of the renewable source variability on systems design. It has been found that the variability increases the difficulty in balancing energy mismatch and it often requires the large excess generation of renewable power to level its output, resulting in large curtailment and increasing costs. This work also analyses two different objectives: (1) minimum storage capacity for a fully renewable operation optimised by excess generation and renewable mix, and (2) the LEC of energy from a renewable power system (including generation and storage) delivered to the MeOH plant, which is optimised by excess generation, renewable mix and storage capacity. It has been found that the renewable mix is important for minimising storage capacity because it allows a complementary renewable source to level their power output, thus reducing the variability in power mismatch. However, for the two selected locations renewable mix has shown no or very little influence on optimising LEC as the costs are primarily determined by the quality of renewable sources. The optimum of both objective functions responds to the change of variables in different ways between the two locations due to the characteristics of their renewable sources.

The correlation between key variables is also explored in this work. In general, the increase in storage size reduces the requirement of dispatchable energy. However, this correlation exhibits a two-regime behaviour where its marginal benefit is significant at the outset but reduces when the storage is larger than 18 (meaning that the production can solely rely on it for 18 hours). This implies the importance of intra-day balancing, especially when solar power dominates the generation. Similarly, in the economic analysis, the renewable penetration (in the most economical scenarios) increases dramatically at the beginning with the increase of dispatchable energy price but levels off when the price is above a critical point. From the economic perspective, both results question the desirability of achieving a fully renewable operation as the required storage capacity and the economic incentive will have to increase significantly. Nevertheless, powering the chemical industry with renewable sources is of significant importance from the viewpoint of industrial decarbonisation.

Acknowledgments

CC thanks the China Scholarship Council and Jesus College, Oxford for financial support.

Supplementary material

Supplementary material associated with this article can be found, in the online version, at [10.1016/j.apenergy.2021.100021](https://doi.org/10.1016/j.apenergy.2021.100021).

References

- [1] Eurostat. Energy balance sheets 2015 data. Dataset; 2017. doi:[102785/032728](https://doi.org/10.2785/032728).
- [2] Kafandaris S. Buying greenhouse insurance: the economic costs of CO₂ emission limits. *J Oper Res Soc* 1994;45(4):479–80. doi:[10.1057/jors.1994.67](https://doi.org/10.1057/jors.1994.67). <https://doi.org/10.1057/jors.1994.67>
- [3] Kempton W, Pimenta FM, Veron DE, Colle BA. Electric power from offshore wind via synoptic-scale interconnection. *Proc Natl Acad Sci* 2010;107(16):7240–5. doi:[10.1073/pnas.0909075107](https://doi.org/10.1073/pnas.0909075107). <https://www.pnas.org/content/107/16/7240>
- [4] Hart EK, Jacobson MZ. A Monte Carlo approach to generator portfolio planning and carbon emissions assessments of systems with large penetrations of variable renewables. *Renew Energy* 2011;36(8):2278–86. doi:[10.1016/j.renene.2011.01.015](https://doi.org/10.1016/j.renene.2011.01.015). <http://www.sciencedirect.com/science/article/pii/S0960148111000371>
- [5] Jacobsen HK, Schröder ST. Curtailment of renewable generation: economic optimality and incentives. *Energy Policy* 2012;49:663–75. doi:[10.1016/j.enpol.2012.07.004](https://doi.org/10.1016/j.enpol.2012.07.004). <http://www.sciencedirect.com/science/article/pii/S030142151200585X>
- [6] Strbac G. Demand side management: benefits and challenges. *Energy Policy* 2008;36(12):4419–26. doi:[10.1016/j.enpol.2008.09.030](https://doi.org/10.1016/j.enpol.2008.09.030). <http://www.sciencedirect.com/science/article/pii/S0301421508004606>
- [7] Samsatli S, Samsatli NJ. The role of renewable hydrogen and inter-seasonal storage in decarbonising heat – comprehensive optimisation of future renewable energy value chains. *Appl Energy* 2019;233–234:854–93. doi:[10.1016/j.apenergy.2018.09.159](https://doi.org/10.1016/j.apenergy.2018.09.159). <http://www.sciencedirect.com/science/article/pii/S0306261918314715>
- [8] Bühler F, Zihlsdorf B, Nguyen T-V, Elmegaard B. A comparative assessment of electrification strategies for industrial sites: case of milk powder production. *Appl Energy* 2019;250:1383–401. doi:[10.1016/j.apenergy.2019.05.071](https://doi.org/10.1016/j.apenergy.2019.05.071). <http://www.sciencedirect.com/science/article/pii/S030626191930916X>
- [9] Schiffer ZJ, Manthiram K. Electrification and decarbonization of the chemical industry. *Joule* 2017;1(1):10–14. doi:[10.1016/j.joule.2017.07.008](https://doi.org/10.1016/j.joule.2017.07.008). <http://www.sciencedirect.com/science/article/pii/S2542435117300156>
- [10] Beerbühl SS, Frhling M, Schultmann F. Combined scheduling and capacity planning of electricity-based ammonia production to integrate renewable energies. *Eur J Oper Res* 2015;241(3):851–62. doi:[10.1016/j.ejor.2014.08.039](https://doi.org/10.1016/j.ejor.2014.08.039). <http://www.sciencedirect.com/science/article/pii/S0377221714007164>
- [11] Heide D, Greiner M, von Bremen L, Hoffmann C. Reduced storage and balancing needs in a fully renewable European power system with excess wind and solar power generation. *Renew Energy* 2011;36(9):2515–23. doi:[10.1016/j.renene.2011.02.009](https://doi.org/10.1016/j.renene.2011.02.009). <http://www.sciencedirect.com/science/article/pii/S0960148111000851>
- [12] Heide D, von Bremen L, Greiner M, Hoffmann C, Speckmann M, Bofinger S. Seasonal optimal mix of wind and solar power in a future, highly renewable Europe. *Renew Energy* 2010;35(11):2483–9. doi:[10.1016/j.renene.2010.03.012](https://doi.org/10.1016/j.renene.2010.03.012). <http://www.sciencedirect.com/science/article/pii/S0960148110001291>
- [13] Rasmussen MG, Andresen GB, Greiner M. Storage and balancing synergies in a fully or highly renewable pan-European power system. *Energy Policy* 2012;51:642–51. doi:[10.1016/j.enpol.2012.09.009](https://doi.org/10.1016/j.enpol.2012.09.009). <http://www.sciencedirect.com/science/article/pii/S0301421512007677>
- [14] Budischak C, Sewell D, Thomson H, Mach L, Veron DE, Kempton W. Cost-minimized combinations of wind power, solar power and electrochemical storage, powering the grid up to 99.9% of the time. *J*

- Power Sources 2013;225:60–74. doi:10.1016/j.jpowsour.2012.09.054. <http://www.sciencedirect.com/science/article/pii/S0378775312014759>
- [15] Ekren O, Ekren BY, Ozerdem B. Break-even analysis and size optimization of a PV/wind hybrid energy conversion system with battery storage a case study. *Appl Energy* 2009;86(7):1043–54. doi:10.1016/j.apenergy.2008.09.024. <http://www.sciencedirect.com/science/article/pii/S0306261908002468>
- [16] Kondratenko EV, Mul G, Baltrusaitis J, Larrazbal GO, Prez-Ram-rez J. Status and perspectives of CO₂ conversion into fuels and chemicals by catalytic, photocatalytic and electrocatalytic processes. *Energy Environ Sci* 2013;6:3112–35. doi:10.1039/C3EE41272E. <https://doi.org/10.1039/C3EE41272E>
- [17] Yarulina I, Chowdhury AD, Meirer F, Weckhuysen BM, Gascon J. Recent trends and fundamental insights in the methanol-to-hydrocarbons process. *Nat Catal* 2018;1(6):398–411. doi:10.1038/s41929-018-0078-5.
- [18] Lonis F, Tola V, Cau G. Assessment of integrated energy systems for the production and use of renewable methanol by water electrolysis and CO₂ hydrogenation. *Fuel* 2021;285:119160. doi:10.1016/j.fuel.2020.119160. <https://www.sciencedirect.com/science/article/pii/S0016236120321566>
- [19] Gonzalez-Garay A, Frei MS, Al-Qahtani A, Mondelli C, Guillen-Gosalbez G, Perez-Ramirez J. Plant-to-planet analysis of CO₂-based methanol processes. *Energy Environ Sci* 2019;12(12):3425–36. doi:10.1039/c9ee01673b.
- [20] Bos M, Kersten S, Brilman D. Wind power to methanol: renewable methanol production using electricity, electrolysis of water and CO₂ air capture. *Appl Energy* 2020;264:114672. doi:10.1016/j.apenergy.2020.114672. <http://www.sciencedirect.com/science/article/pii/S0306261920301847>
- [21] Nguyen TB, Zondervan E. Methanol production from captured CO₂ using hydrogenation and reforming technologies - environmental and economic evaluation. *J CO₂ Util* 2019;34:1–11. doi:10.1016/j.jcou.2019.05.033. <http://www.sciencedirect.com/science/article/pii/S2212982019300320>
- [22] Shaner MR, Atwater HA, Lewis NS, McFarland EW. A comparative technoeconomic analysis of renewable hydrogen production using solar energy. *Energy Environ Sci* 2016;9:2354–71. doi:10.1039/C5EE02573G. <https://doi.org/10.1039/C5EE02573G>
- [23] Perez-Fortes M, Schoneberger JC, Boulamanti A, Tzimas E. Methanol synthesis using captured CO₂ as raw material: techno-economic and environmental assessment. *Appl Energy* 2016;161:718–32. doi:10.1016/j.apenergy.2015.07.067. <Go to ISI> ://WOS:000366063100060
- [24] Esteves N, Sigal A, Leiva E, Rodriguez C, Cavalcante F, de Lima L. Wind and solar hydrogen for the potential production of ammonia in the state of Cear Brazil. *Int J Hydrog Energy* 2015;40(32):9917–23. doi:10.1016/j.ijhydene.2015.06.044. <http://www.sciencedirect.com/science/article/pii/S0360319915015293>
- [25] Chen C, Lu Y, Bñares-Alcántara R. Direct and indirect electrification of chemical industry using methanol production as a case study. *Appl Energy* 2019;243:71–90. doi:10.1016/j.apenergy.2019.03.184. <http://www.sciencedirect.com/science/article/pii/S0306261919306002>
- [26] Beaudin M, Zareipour H, Schellenberg A, Rosehart W. Energy storage for mitigating the variability of renewable electricity sources: an updated review. *Energy Sustain Dev* 2010;14(4):302–14. doi:10.1016/j.esd.2010.09.007. <http://www.sciencedirect.com/science/article/pii/S0973082610000566>
- [27] Zeng K, Zhang D. Recent progress in alkaline water electrolysis for hydrogen production and applications. *Prog Energy Combust Sci* 2010;36(3):307–26. doi:10.1016/j.pecs.2009.11.002. <http://www.sciencedirect.com/science/article/pii/S0360128509000598>
- [28] Wang C. Modeling and control of hybrid wind/photovoltaic/fuel cell distributed generation systems. Montana State University; 2006. Thesis.
- [29] Wang G, Mitsos A, Marquardt W. Conceptual design of ammonia-based energy storage system: system design and time-invariant performance. *AIChE J* 2017;63(5):1620–37. doi:10.1002/aic.15660. <https://aiche.onlinelibrary.wiley.com/doi/abs/10.1002/aic.15660>
- [30] Zhang C, Jun K-W, Gao R, Kwak G, Park H-G. Carbon dioxide utilization in a gas-to-methanol process combined with CO₂/steam-mixed reforming: techno-economic analysis. *Fuel* 2017;190:303–11. doi:10.1016/j.fuel.2016.11.008. <http://www.sciencedirect.com/science/article/pii/S0016236116311024>
- [31] Vestas Wind Systems. General specification for V90 3.0 MW: 60 Hz variable speed turbine. Report; 2004.
- [32] Matzen M, Alhajji M, Demirel Y. Chemical storage of wind energy by renewable methanol production: Feasibility analysis using a multi-criteria decision matrix. *Energy* 2015;93:343–53. doi:10.1016/j.energy.2015.09.043. <http://www.sciencedirect.com/science/article/pii/S03060544215012530>
- [33] Nayak-Luke R, Baares-Alcántara R, Wilkinson I. Green ammonia: impact of renewable energy intermittency on plant sizing and levelized cost of ammonia. *Ind Eng Chem Res* 2018;57(43):14607–16. doi:10.1021/acs.iecr.8b02447. <https://doi.org/10.1021/acs.iecr.8b02447>
- [34] Steward D. Scenario development and analysis of hydrogen as a large-scale energy storage medium. Report. National Renewable Energy Laboratory; 2009.
- [35] Peters R, Deja R, Engelbracht M, Frank M, Nguyen VN, Blum L, et al. Efficiency analysis of a hydrogen-fueled solid oxide fuel cell system with anode off-gas recirculation. *J Power Sources* 2016;328:105–13. doi:10.1016/j.jpowsour.2016.08.002. <https://www.sciencedirect.com/science/article/pii/S0378775316310011>
- [36] Eurostat. Electricity price statistics. Report; 2017. doi:10.2785/032728.
- [37] Chen C. Using dispatchable energy price as a tool to predict and influence the renewable penetration in chemical production. In: Proceedings of the 23rd Conference on Process Integration, Modelling and Optimisation for Energy Saving and Pollution Reduction; 2020.
- [38] Tountas AA, Peng X, Tavasoli AV, Duchesne PN, Dingle TL, Dong Y, et al. Towards solar methanol: past, present, and future. *Adv Sci* 2019;6(8):1801903. doi:10.1002/adv.201801903. <https://onlinelibrary.wiley.com/doi/abs/10.1002/adv.201801903>
- [39] Moro A, Lonza L. Electricity carbon intensity in European member states: impacts on GHG emissions of electric vehicles. *Transp Res Part D Transp Environ* 2018;64:5–14. doi:10.1016/j.trd.2017.07.012. <http://www.sciencedirect.com/science/article/pii/S1361920916307933>
- [40] US Energy Information Administration. Monthly energy review December 2019. Report; 2019.
- [41] Gielen D, Boshell F, Gorini R, Kiruja J, Komor P, Masuyama T, et al. Renewable power generation costs in 2019 Report. International Renewable Energy Agency; 2020.
- [42] Chen C, Yang A. Power-to-methanol: the role of process flexibility in the integration of variable renewable energy into chemical production. *Energy Convers Manag* 2021;228:113673. doi:10.1016/j.enconman.2020.113673. <http://www.sciencedirect.com/science/article/pii/S0196890420311997>
- [43] Kajaste-Rudnitskaja R, Hurme M, Oinas P. Methanol-managing greenhouse gas emissions in the production chain by optimizing the resource base. *AIMS Energy* 2018;6:1074–102. doi:10.3934/energy.2018.6.1074. <http://urn.fi/URN:NBN:fi:aalto-201904022426>
- [44] Ekren O, Ekren BY. Size optimization of a PV/wind hybrid energy conversion system with battery storage using simulated annealing. *Appl Energy* 2010;87(2):592–8. doi:10.1016/j.apenergy.2009.05.022. <http://www.sciencedirect.com/science/article/pii/S0306261909002177>
- [45] Boyle G. Renewable energy: power for a sustainable future. Oxford University Press; 2004. p. 55–6.
- [46] Esposito DV. Membraneless electrolyzers for low-cost hydrogen production in a renewable energy future. *Joule* 2017;1(4):651–8. doi:10.1016/j.joule.2017.07.003. <http://www.sciencedirect.com/science/article/pii/S2542435117300107>
- [47] Nayak-Luke RM, Bñares-Alcántara R. Techno-economic viability of islanded green ammonia as a carbon-free energy vector and as a substitute for conventional production. *Energy Environ Sci* 2020;13:2957–66. doi:10.1039/D0EE01707H. <https://doi.org/10.1039/D0EE01707H>
- [48] Celik AN. Techno-economic analysis of autonomous PV-wind hybrid energy systems using different sizing methods. *Energy Convers Manag* 2003;44(12):1951–68. doi:10.1016/S0196-8904(02)00223-6. <http://www.sciencedirect.com/science/article/pii/S0196890402002236>
- [49] Hank C, Gelpke S, Schnabl A, White RJ, Full J, Wiebe N, et al. Economics & carbon dioxide avoidance cost of methanol production based on renewable hydrogen and recycled carbon dioxide power-to-methanol. *Sustain Energy Fuels* 2018;2:1244–61. doi:10.1039/C8SE00032H. <https://doi.org/10.1039/C8SE00032H>
- [50] Bñares-Alcántara R, Dericks III G, Fiaschetti M, Grnewald P, Lopez JM, Tsang E, et al. Analysis of islanded ammonia-based energy storage systems Report. University of Oxford; 2015.
- [51] Baronia R, Goel J, Gautam G, Singh D, Singhal SK. Synthesis and characterization of nitrogen doped reduced graphene oxide (N-rGO) supported PtCu anode catalysts for direct methanol fuel cell. *J Nanosci Nanotechnol* 2019;19(7):3832–43.